9 Essential Concepts on Ultrasonography of Skin Cancer

Ximena Wortsman, Kharla Pizarro, Yamile Corredoira, Laura Carreño, and Claudia Morales

Introduction

One of the main advantages of ultrasound is the possibility of evaluating skin cancer [1–5]. The role of ultrasound is to support the detection of the primary tumor and its extent in all axes, including depth, as well as the performance of locoregional staging [1–6]. This is relevant because, so far, ultrasound is the only imaging technique that can define the depth of the tumor without penetration issues [1–7]. In contrast, dermoscopy, confocal microscopy, and optical coherence tomography are limited by the penetration of the light that can make difficult the observation of the deep border in tumors thicker than 200 μ or 2 mm according to the technique [1–3]. On the other hand, PET-CT and MRI present a lower axial spatial resolution in comparison with ultrasound at ≥15 MHz [1–3, 8–10]. The latter point is relevant because not all ultrasound devices are useful for performing studies of the primary tumor or their locoregional staging. Indeed, there are minimum requirements for performing the examinations, including a proper device and a trained operator [11, 12]. The lack of these factors may decrease the sensitivity of the detection [11, 12]. Moreover, the quality of the ultrasound devices is also an important point because devices older than 5 years may not be comparable with new machines. These features may explain why some reviews or reports do not consider ultrasound as an accurate imaging modality for studying skin cancer. Usually, in these cases, there are non-recommended or unclear ultrasound devices and a lack of trained operators [13].

Thus, to date, ultrasound is the first imaging modality to observe and measure the primary tumor, including all axes, and perform a locoregional staging [1–3, 6, 14, 15].

Skin cancers can be separated into non-melanoma and melanoma [3, 4, 6]. The most common non-melanoma skin cancers are basal cell carcinoma and squamous cell carcinoma [3, 4, 6]. Other less common types of non-melanoma tumors include dermatofibrosarcoma protuber-

X. Wortsman (✉)
Institute for Diagnostic Imaging and Research of the Skin and Soft Tissues, Santiago, RM, Chile

Department of Dermatology, Universidad de Chile, Santiago, RM, Chile

Department of Dermatology, Pontificia Universidad Catolica de Chile, Santiago, RM, Chile

K. Pizarro
Department of Pathology, Hospital San José, Santiago, Chile

Y. Corredoira
Department of Pathology, Hospital San Borja Arriaran, Central Campus Faculty of Medicine, Universidad de Chile, Santiago, Chile

L. Carreño · C. Morales
Department of Pathology, Dermopathology Section, Universidad de Chile, Santiago, Chile

X. Wortsman (ed.), *Textbook of Dermatologic Ultrasound*,
https://doi.org/10.1007/978-3-031-08736-3_9

ans, cutaneous lymphomas, Merkel cell tumors, and liposarcomas [3, 4].

Even though the most common types of non-melanoma skin cancers are usually not lethal, they can generate important disfiguration and strongly affect the self-esteem of individuals [1–4, 16].

This chapter reviews essential concepts on the ultrasonographic appearance of skin cancer following a practical approach and combining the clinical, ultrasonographical, and histologic features.

Non-melanoma Skin Cancers

Basal Cell Carcinoma (BCC)

Also called basal cell epithelioma or basalioma, this is the most common skin cancer in humans and commonly affects the sun-exposed regions such as the face in 85% of cases [1–4, 16–19]. On ultrasound, BCC shows a hypoechoic oval or band-like lesion that frequently presents hyperechoic spots and affects the dermis and sometimes the hypodermis and deeper layers [1–4, 6, 14, 16, 18–33]. Other less frequent forms of presentation are the asymmetric, hourglass, bulging, butterfly, or irregular shapes [16].

The presence of hyperechoic spots is a vital sign for diagnosing BCC because they have not been reported in squamous cell carcinoma or melanoma. These hyperechoic spots are linked to the risk of recurrence of the BCC histologic subtype [16, 31, 33]. Thus, hyperechoic spots are higher in number ($\geq$7) in the more aggressive subtypes such as micronodular, morpheaform, sclerosing, metatypical, and infiltrative [33].Low-risk-of-recurrence histologic subtypes include macronodular or nodular, superficial, adenoid cystic, and Pinkus fibroepithelioma [33].

Even though some of these hyperechoic spots correspond to calcium deposits and corneum cysts, the majority are not detected in the histological samples studied with hematoxylin and eosin; therefore, it is thought that they are compact nests of neoplastic cells or molecular deposits that generate this ultrasonographic pattern [33]. In dermoscopy, there are multiple aggregates of yellow-white globules in nonpigmented BCC that perhaps may be linked to the hyperechoic spots because a high number of aggregates of yellow-white globules have been reported in high-risk-of-recurrence histologic subtypes of BCC [34].

These hyperechoic spots may also be detected in some cases of trichoepithelioma, a close lesion to BCC [4]. Additionally, the calcifications of chondroid syringomas may present a differential diagnosis, but chondroid syringomas show other morphology and tend to be close to cartilage.

It is not uncommon to find mixed tumors that contain a low- and high-risk-of-recurrence tumors in the same lesion [35]. In these cases, ultrasound can support selecting the best biopsy site besides supporting the diagnosis.

On color Doppler ultrasound, their vascularity is variable and can range from hypovascular to intermediate degree of vascularity [16]. In some cases, there is inflammation surrounding the BCC lesions that may generate a minor overestimation of the size [21], which is, of course, lower when ultrahigh frequency probes such as 70 MHz are used.

The ultrasonographic detection of involvement of deeper layers in BCC is of paramount importance, particularly in the facial lesions that can easily extend into the muscles, such as the orbicularis muscles of the eyelids or the lips and the nasal cartilages. This information is critical for surgical planning because the objective is to provide both oncological and cosmetic good results (Figs. 9.1, 9.2, 9.3, and 9.4) [1–4, 30–33, 35].

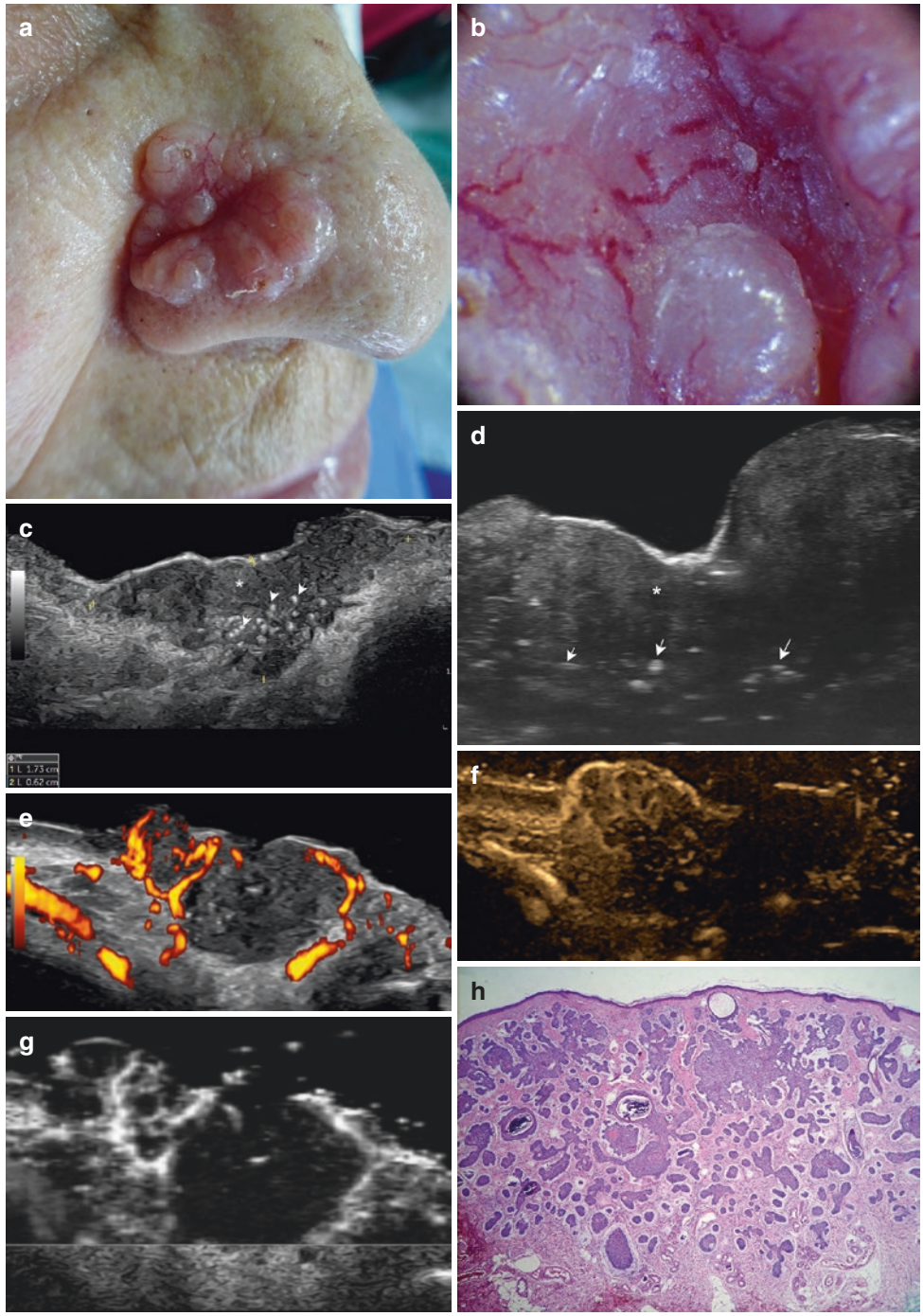

Fig. 9.1 Basal cell carcinoma (high-risk-of-recurrence subtype). (**a**) Photography and (**b**) dermoscopy of the clinical lesion. Ultrasound images (**c** and **d**, grayscale; **c** at 24 MHz and **d** at 70 MHz; **e**, power Doppler; **f**, echoangio; and **g**, microvascular imaging; transverse view) demonstrate 1.73 cm (transverse) × 0.62 cm (depth), ill-defined hypoechoic dermal and subcutaneous lesion (*) with multiple hyperechoic spots (*) in the deep part. Notice the internal vascularity in **f**,**g**. (**h**) Histology (H&E 40X): basaloid cellular proliferation arranged in medium and small nests. The tumor nests extend to the papillary and reticular dermis. There are some areas of calcification within nests of basal cell carcinoma

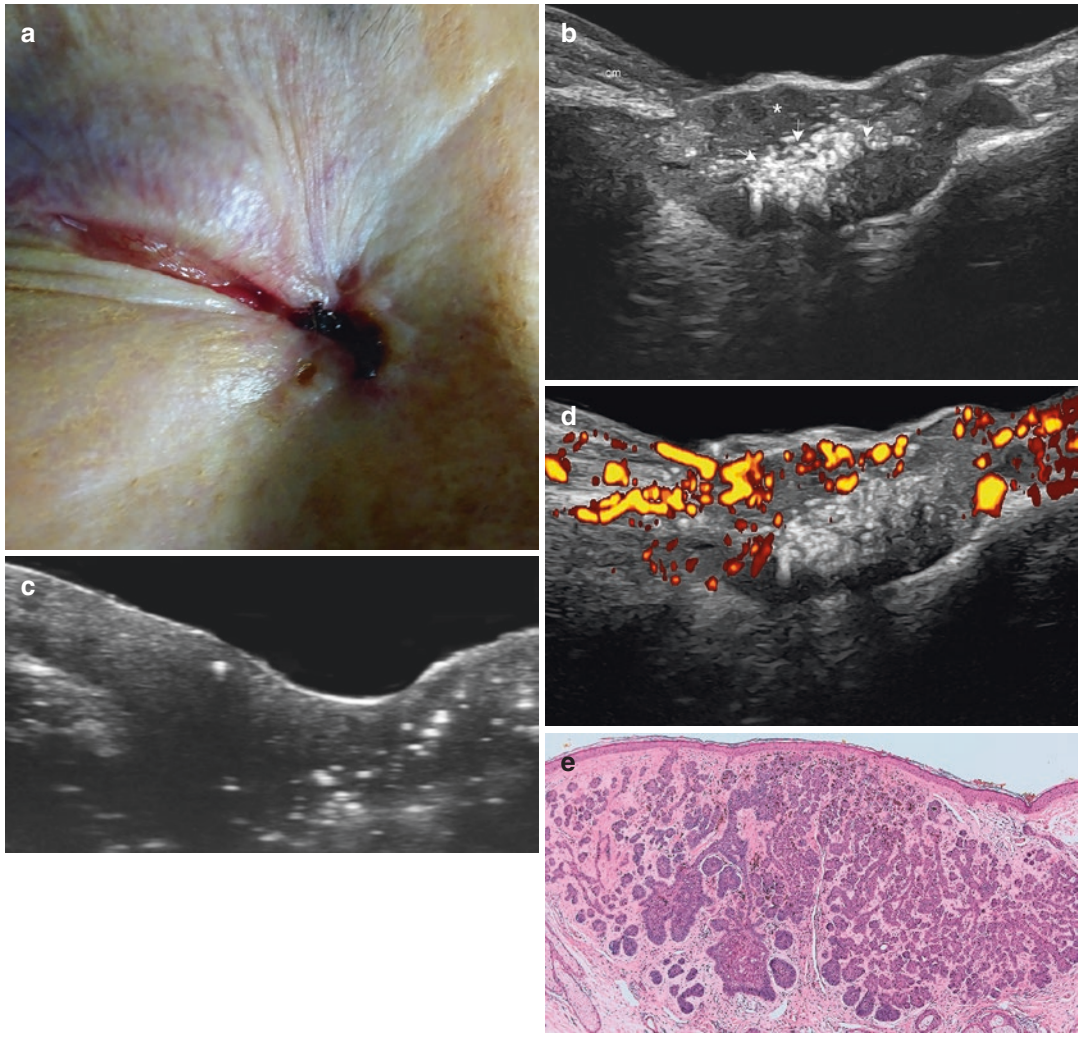

Fig. 9.2 Basal cell carcinoma (high-risk-of-recurrence subtype). (**a**) Clinical image. Ultrasound images (**b** and **d**, grayscale; **b** at 24 MHz, **c** at 70 MH, and **d**, power Doppler ultrasound; transverse view) present ill-defined hypoechoic dermal and subcutaneous lesion (*) with multiple hyperechoic spots (arrows) and with involvement of the medial part of the orbicularis oculi muscle (om). (**e**) Histology (H&E 50x): proliferation of medium and small basaloid nests in the papillary and reticular dermis. Some nodules show peripheral palisading and clefting, and melanin pigment

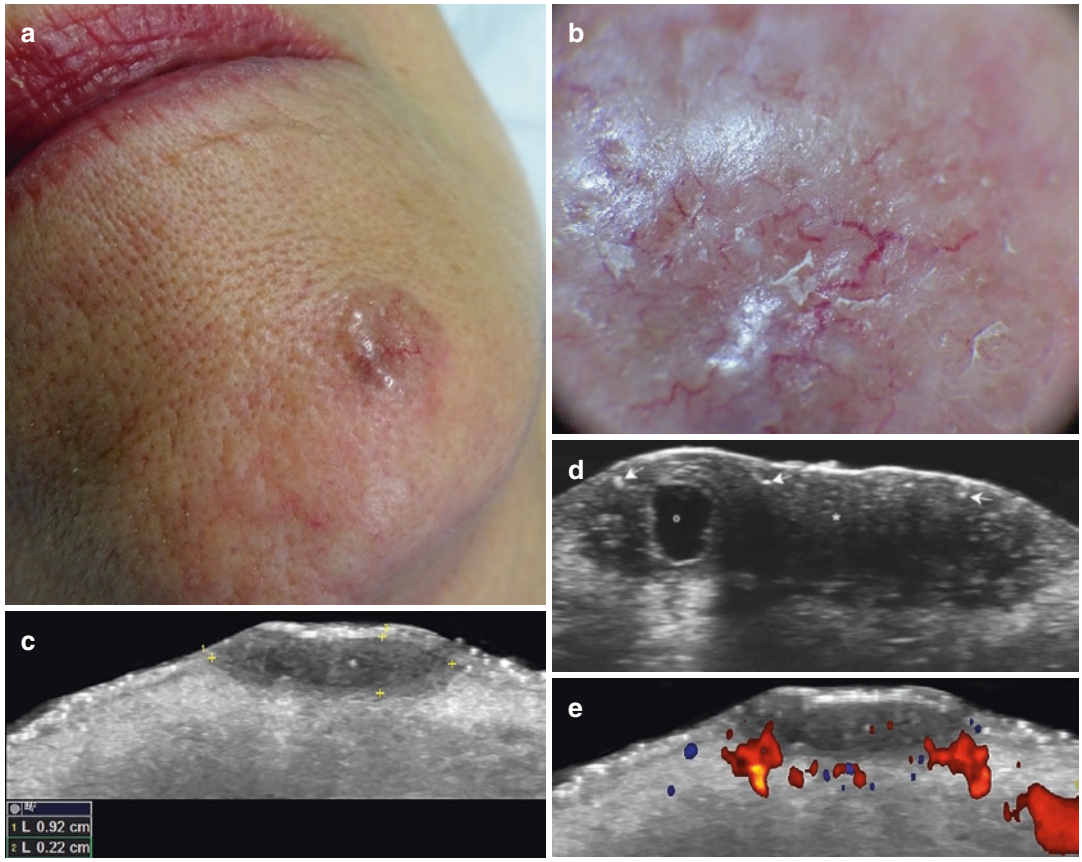

Fig. 9.3 Basal cell carcinoma (low-risk-of-recurrence subtype). (**a**) Clinical photograph and (**b**) dermoscopy of the lesion. Ultrasound images (**c** and **d** grayscale and **e** color Doppler; transverse view) show 0.92 cm (transverse) x 0,22 cm (depth) hypoechoic dermal lesion (*, between markers in **c**). Notice isolated hyperechoic spots (arrows), an anechoic pseudocystic area (o), and a low degree of hypervascularity that predominates in the sublesional region (see **e**)

Squamous Cell Carcinoma (SCC)

Also called spinocellular carcinoma, epithelioma spinocellular, and spinalioma, this tumor is less frequent than BCC but commonly affects similar corporal regions such as the face or the scalp [3, 4, 6, 28, 36]. On ultrasound, they present as focal oval or a band-like hypoechoic dermal structure that can infiltrate the hypodermis and deeper layers and may present lobulated or irregular borders [3, 4, 6, 28, 36]. Commonly, they present epidermal irregularities and thickening. The involvement of muscle and cartilages is more common in SCC in comparison with BCC [3, 4, 6, 36]. Despite the lack of guidelines for studying SCC, performing a locoregional staging in these cases would be relevant because their more aggressive nature can even involve the regional lymph nodes.

Occasionally, SCCs may appear in scar sites and under immunosuppressive conditions, affecting sun-non-exposed corporal regions.

On color Doppler, SCC shows a variable degree of vascularity, but they tend to be more hypervascular than BCCs (Figs. 9.5, 9.6, and 9.7) [3, 4, 6, 36].

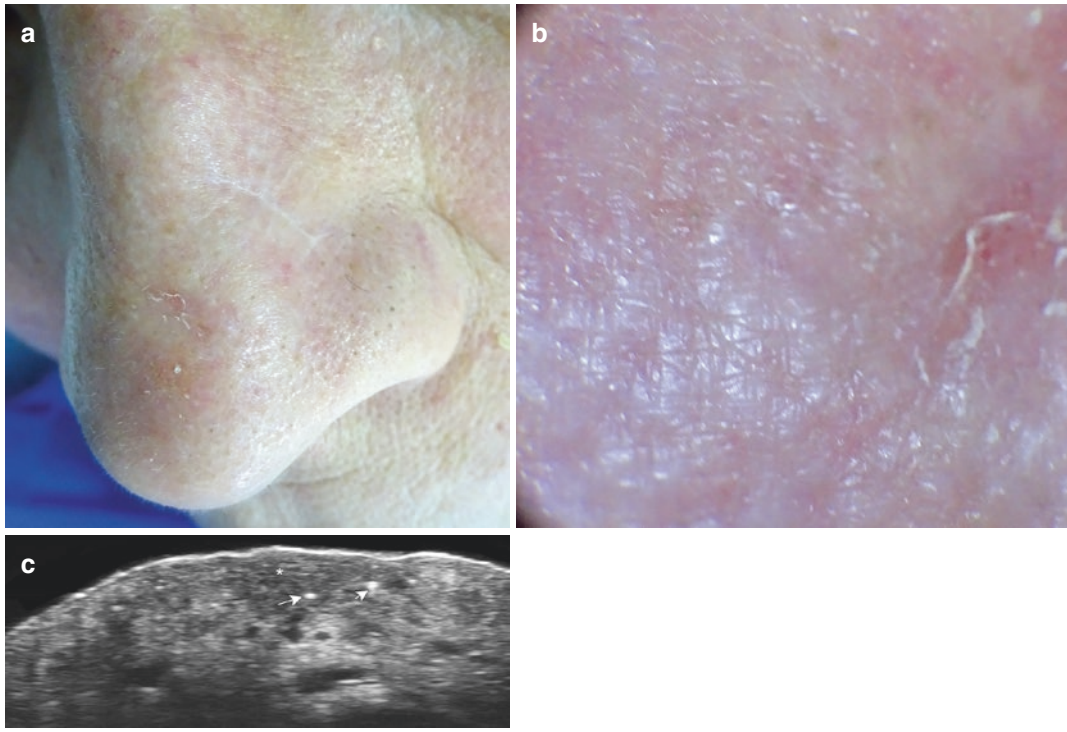

Fig. 9.4 Basal cell carcinoma (low-risk-of-recurrence subtype) (**a**) Clinical photograph and (**b**) dermoscopy of the lesion. (**c**) Ultrasound image (grayscale transverse view) demonstrates an ill-defined hypoechoic dermal lesion (*) with few hyperechoic spots (arrows)

Dermatofibrosarcoma Protuberans (DFSP)

This fibrous sarcomatous tumor presents high local recurrence rates and a low risk of metastases [37]. On ultrasound, DFSP generates ill-defined, mixed echogenicity lesions with a dermal hypoechoic cap and hyperechoic pseudopods and sometimes with lobulated borders that infiltrate the hypodermis [3, 4, 38, 39]. DFSP presents ill-defined borders and displaces the epidermis upward, generating a pseudonodular appearance in some cases. Satellite hypoechoic nodules may be detected in the periphery of the primary tumor [3, 4, 38, 39].

DFSP presents an intermediate degree of vascularity on color Doppler ultrasound with low-flow arterial and/or venous vessels (Figs. 9.8, 9.9, and 9.10) [3, 4].

Merkel Cell Tumor

These aggressive malignant neuroendocrine tumors derive from Merkel cells, usually affect older people, and are commonly located in the head. It has a high incidence of local recurrence as well as nodal and distant metastatic disease [40–43].

The 5-year survival rates are 64% for local disease, 39% for regional nodal involvement, and 18% for distant metastatic disease [42, 43].

On ultrasound, they show as hypoechoic dermal or deeper lesions commonly bulging and highly hypervascular with low-velocity arterial vessels. It is essential to assess the involvement of deeper layers in these cases because it is not uncommon (Fig. 9.11) [40, 41, 44, 45].

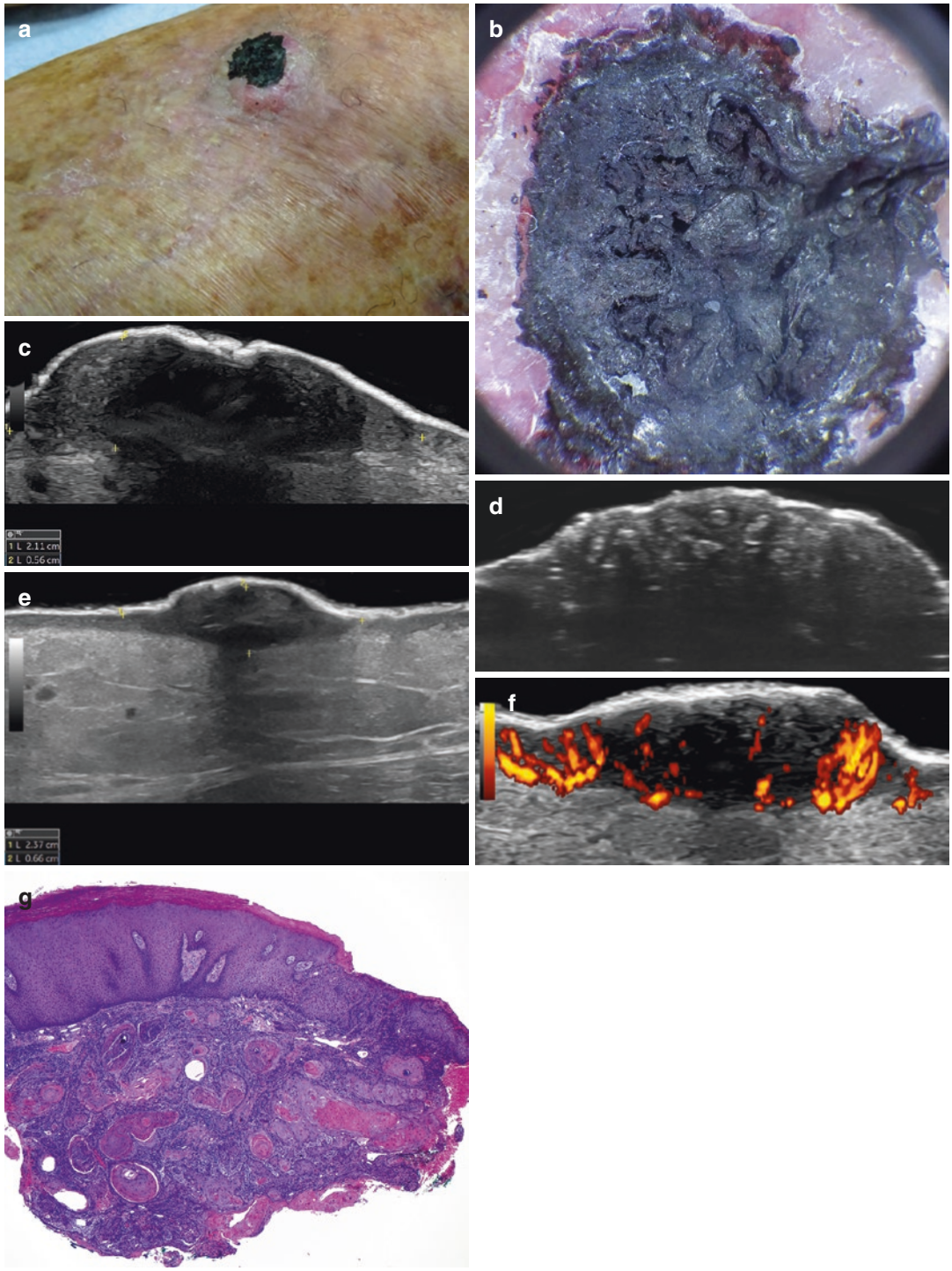

Fig. 9.5 Squamous cell carcinoma. (**a**) Clinical image and (**b**) dermoscopy of the lesion located in the anterior aspect of the right leg. Ultrasound images (**c**–**e**, grayscale; **f**, power Doppler; longitudinal views) present 2.37 cm (long) × 0.66 cm (depth) hypoechoic and heterogeneous dermal lesion with epidermal thickening and irregularities. On power Doppler (**f**), there is prominent vascularity within the lesion. (**g**) Histology (H&E 25X): hyperplastic epidermis overlying dermis with numerous infiltrating masses of keratinizing eosinophilic epithelium. Note concentric keratinization characteristic of well-differentiated squamous cell carcinoma

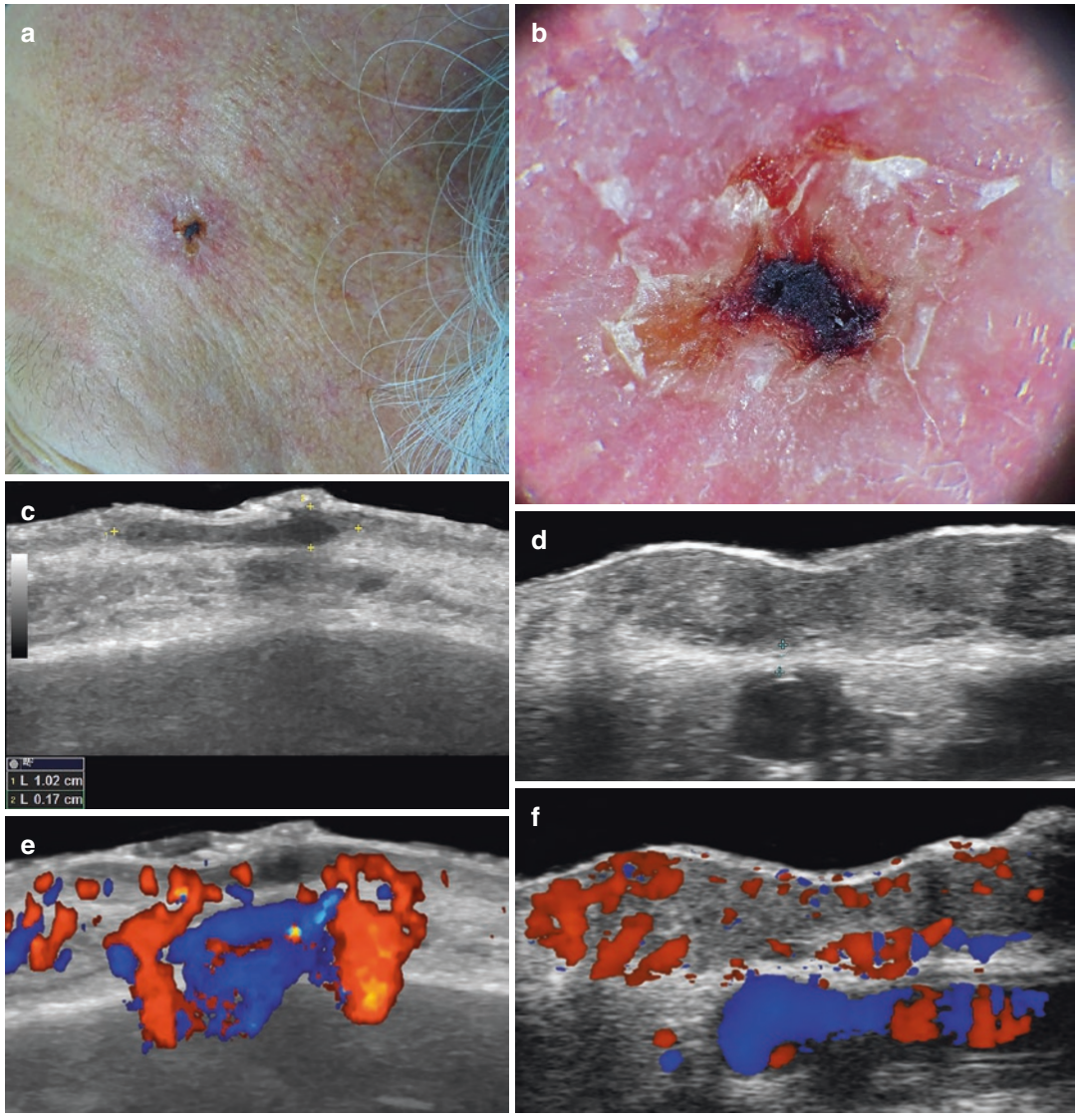

Fig. 9.6 Squamous cell carcinoma. (**a**) Clinical image and (**b**) dermoscopy of a lesion in the left frontal region. Ultrasound images (**c** and **d**, grayscale, **c** at 18 MHz and **d** at 70 MHz; **e** and **f**, color Doppler, **e**, at 18 MHz and **f**, at 70 MHz) demonstrate hypoechoic dermal lesion with epidermal thickening and undulation. On color Doppler, there is prominent vascularity within the lesion

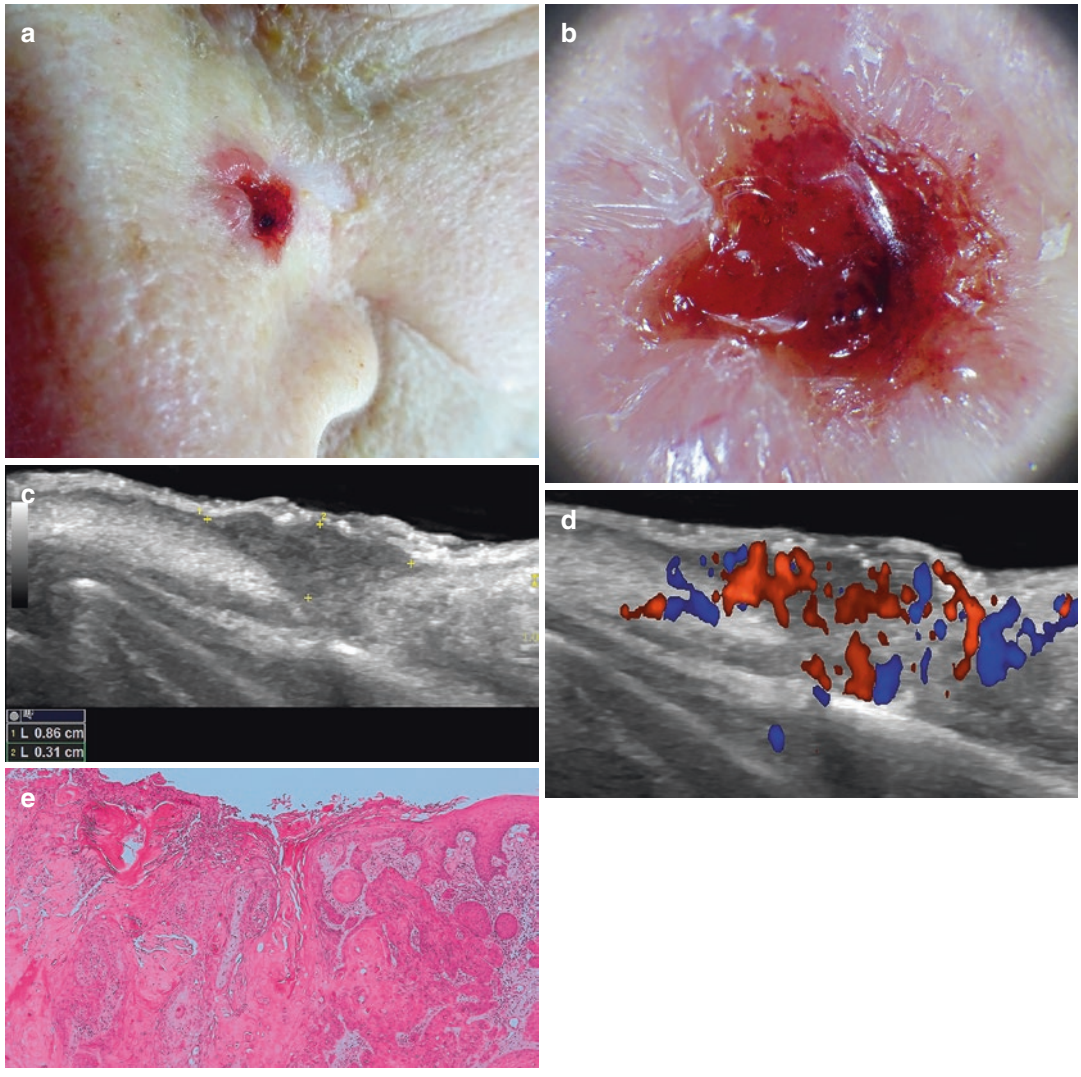

Fig. 9.7 Squamous cell carcinoma. (**a**) Clinical and (**b**) dermoscopy view of lesion located in the left nasal region. Ultrasound images (**c**, grayscale and **d**, color Doppler ultrasound, transverse views) present 0.86 cm (transverse) × 0.31 cm (depth) dermal and subcutaneous hypoechoic lesion (between markers) that shows ill-defined borders, epidermal thickening, and irregularities. On color Doppler, there is hypervascularity within the lesion and its periphery. (**e**) Histology H&E 50x: nests of squamous epithelial cells arising from the epidermis and extending into the dermis. Malignant cells are large with abundant eosinophilic cytoplasm

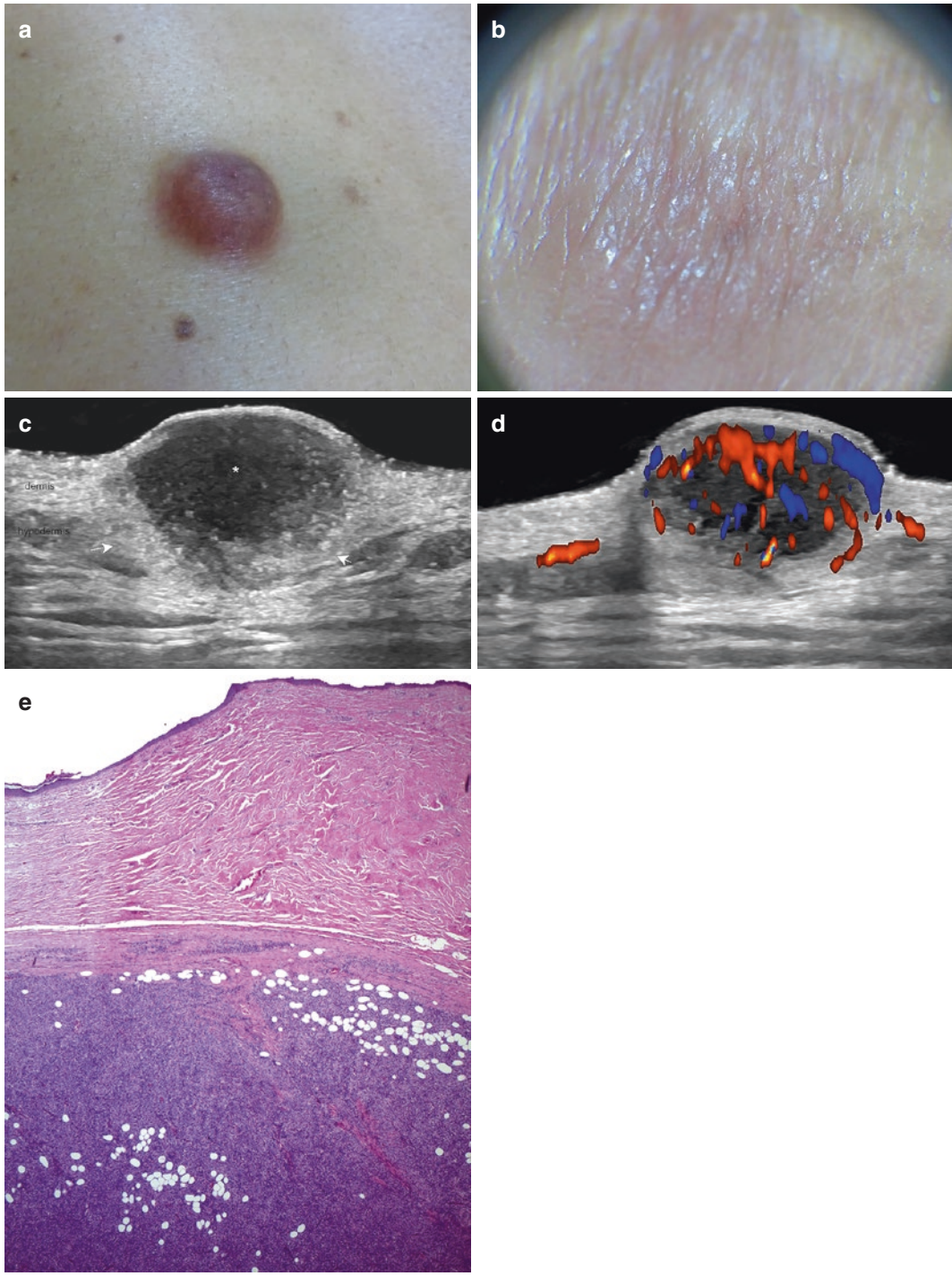

Fig. 9.8 Dermatofibrosarcoma protuberans. (**a**) Clinical and (**b**) dermoscopy image of the lesion. Ultrasound images (**c** and **d**; **c**, grayscale and **d**, color Doppler; transverse views) present hypoechoic dermal lesion (*) with ill-defined borders that displaces the epidermis upward and shows hyperechogenicity with ill-defined borders (arrows) of the underlying hypodermis. On color Doppler, there is hypervascularity within the lesional area. (**e**) Histology (H&E 25X): infiltrative solid spindle cell proliferation in the deep dermis and subcutaneous fat. Infiltration of hypodermal adipose tissue generates a lace-like appearance with some adipocytes well outlined by neoplastic cells

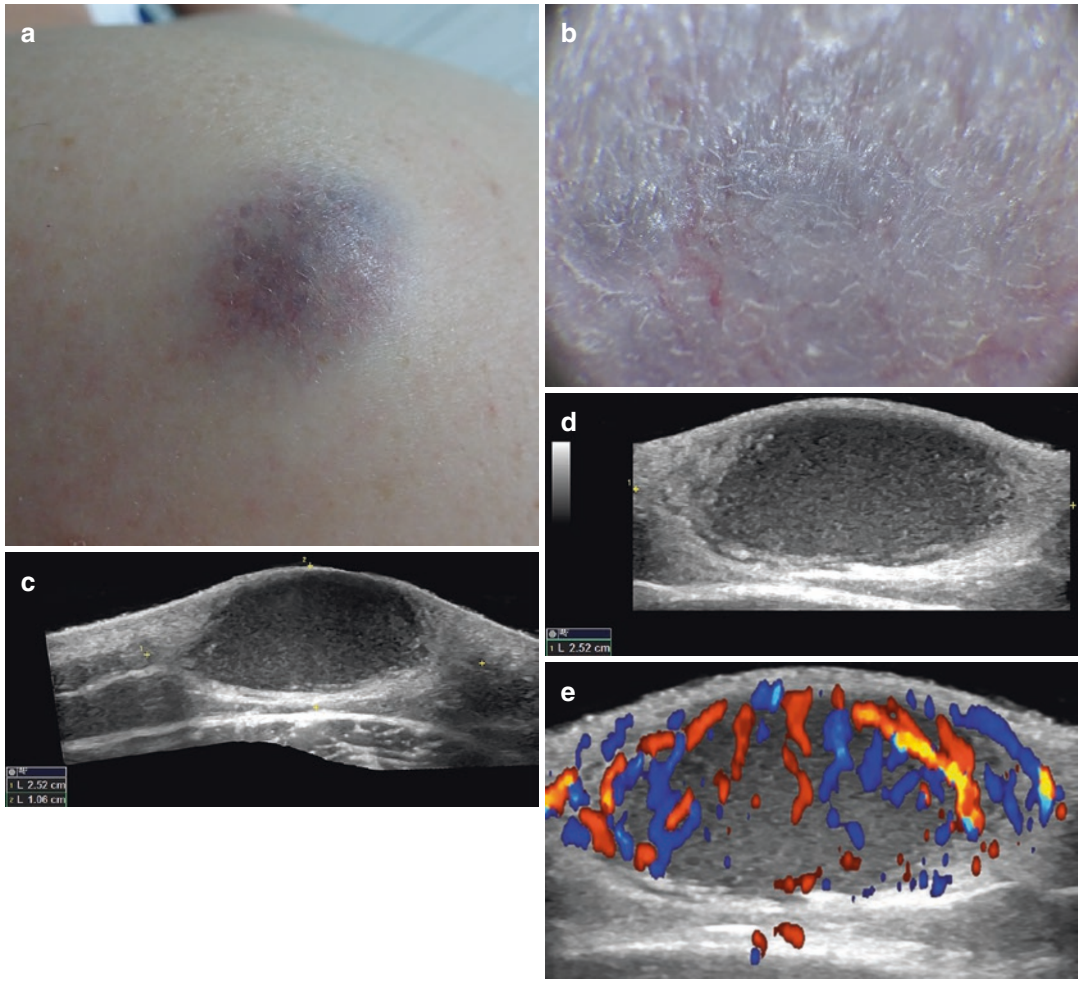

Fig. 9.9 Dermatofibrosarcoma protuberans. (**a**) Clinical photograph and (**b**) dermoscopy of a lesion located in the right shoulder. Ultrasound images (**c** and **d**, grayscale; **c** panoramic view; **d**, zoom view; **e**, color Doppler) show 2.52 cm (transverse) × 1.06 cm (depth) hypoechoic dermal and hypodermal lesion. Notice the ill-defined and slightly lobulated borders as well as the hyperechogenicity of the hypodermal part of the structure. On color Doppler, the lesion presents internal hypervascularity

Primary Cutaneous Lymphomas

Primary cutaneous lymphomas (PCL) are the second most common extranodal non-Hodgkin lymphomas, and their estimated annual incidence is 1/100,000 in Western countries. PCL differ significantly from nodal lymphomas and primary extranodal lymphomas in other locations because they tend to remain localized to the skin for a long time with a much more indolent course and a much better prognosis than lymphomas of similar histological subtype in other locations.

According to their origin, they can be classified into T cell, B cell, and natural killer (NK) cell. Cutaneous T cell lymphomas (CTCL) are the most frequent type and account for approximately 75–80% of all lymphomas, comprising a heterogeneous group [46–52].

Among CTCL, mycosis fungoides (MF) is the most common subtype and accounts for approxi-

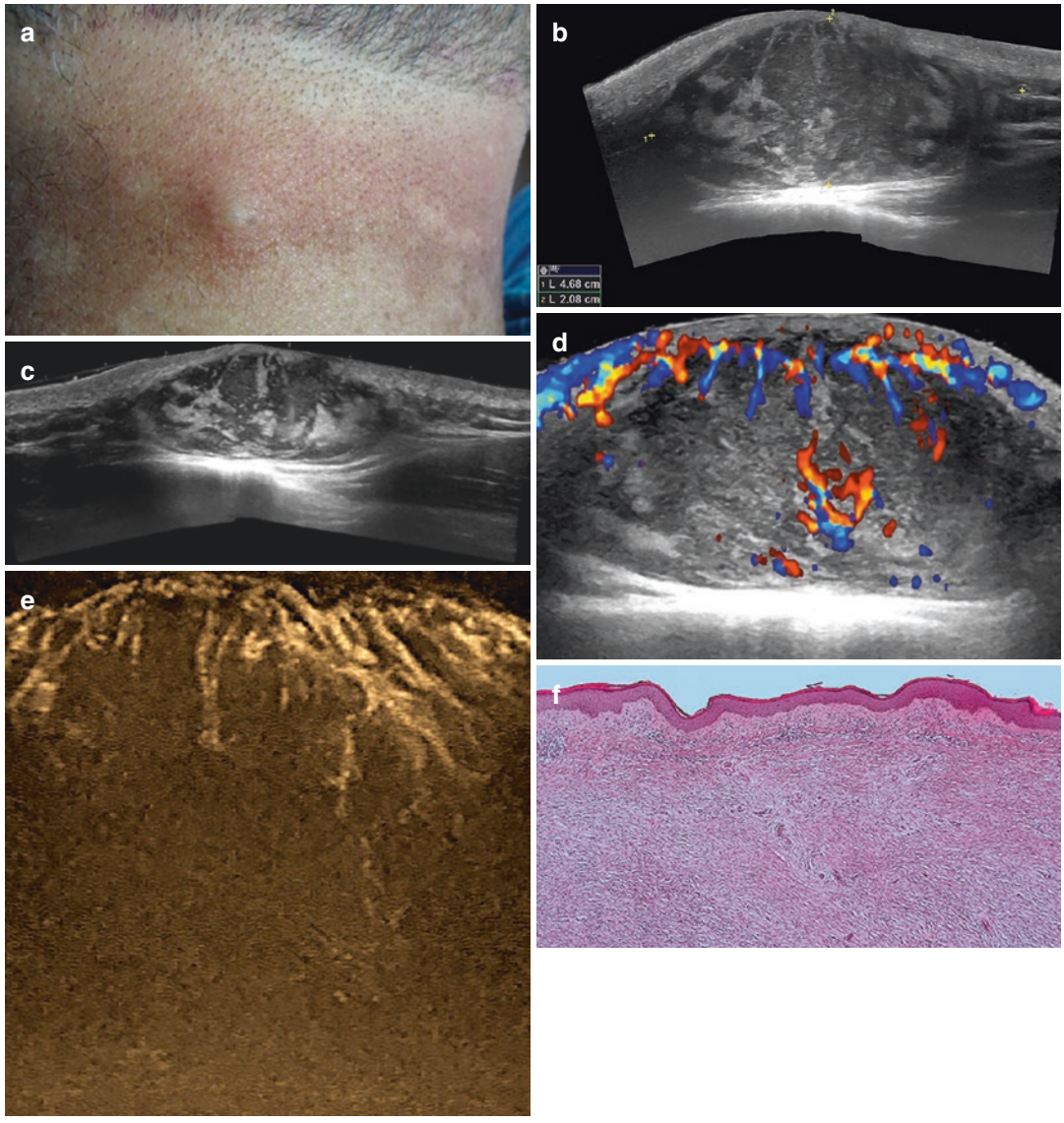

Fig. 9.10 Dermatofibrosarcoma protuberans. (**a**) Clinical photograph of lesion located in the posterior aspect of the neck. Ultrasound images (**b** and **c**, grayscale; **d**, color Doppler; and **e**, echoangio) demonstrate 4.68 (transverse) × 2.08 cm (depth) dermal and hypodermal heterogeneous structure. On color Doppler and echoangio, notice the inner and peripheral hypervascularity of the structure. (**f**) Histology (H&E 50x): poorly circumscribed neoplasm comprised of the monomorphous proliferation of spindle cells in the dermis

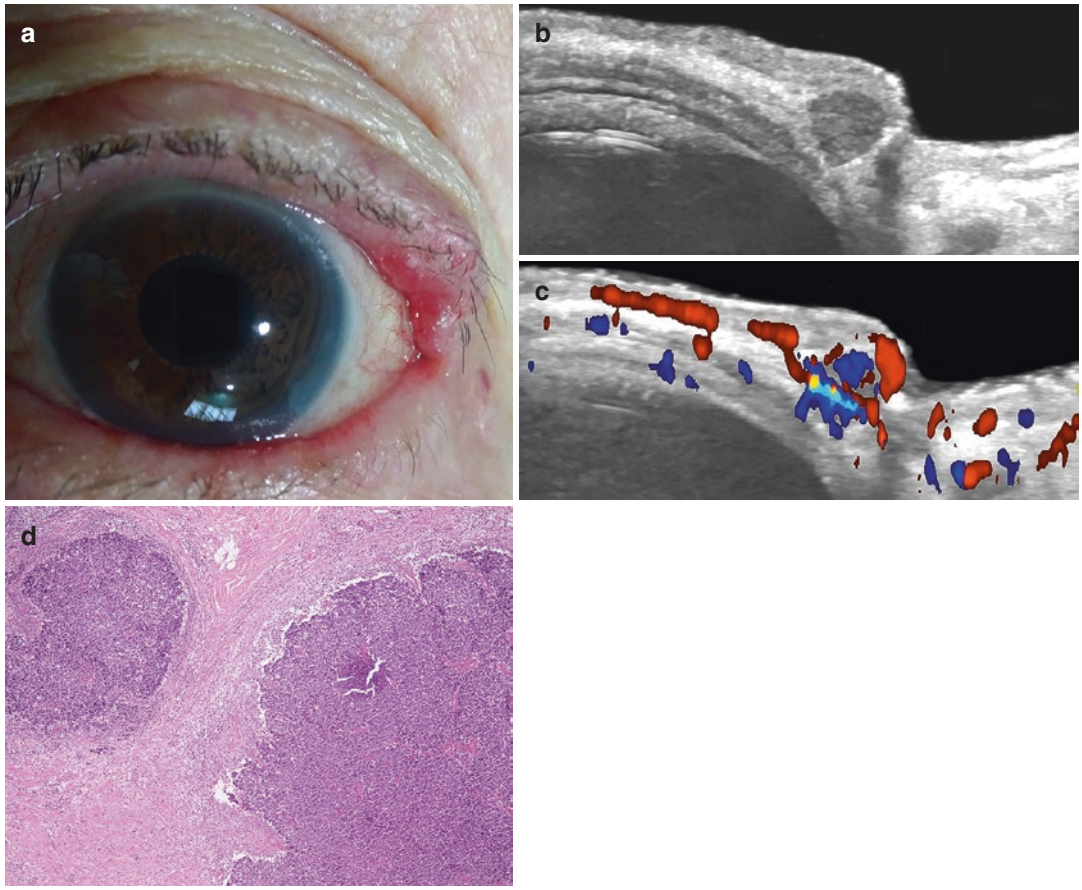

Fig. 9.11 Merkel cell tumor. (**a**) Clinical image of a lesion located in the upper eyelid. Ultrasound images (**b**, grayscale and **c**, color Doppler; longitudinal views) present hypoechoic dermal and intramuscular hypoechoic and hypervascular nodule protruding into the tarsal plate of the eyelid. (**d**) Histology (H&E, 40x): nodular infiltrative tumor within the dermis of monotonous round tumor cells. The tumor cells are basophilic, with round hyperchromatic nuclei and finely granular chromatin with a high nuclear-to-cytoplasmic ratio

mately 80%. MF originates in the peripheral epidermotropic T cells, specifically the memory T cells (CD45RO+), which express the T-cell receptor (TCR) and CD4+ immunophenotype. There are less frequent subtypes, such as folliculotropic MF (FMF), in which the malignant T cells infiltrate the hair follicle epithelium [46, 47, 49–53].

Primary cutaneous B-cell lymphomas (pCBCL) include an infrequent group of non-Hodgkin lymphomas that are limited to skin sites at the time of diagnosis. This type of lymphoma accounts for approximately 25% and is composed of several subtypes [48, 50–52].

Subcutaneous panniculitis-like T-cell lymphoma (SPTCL) is a rare primary cutaneous lymphoma composed of cytotoxic alpha-beta T cells that mimics panniculitis [54].

Clinically, they can show plaques, papules, and nodules to mixed cutaneous lesions, from erythematous to violaceous [52, 55].

On ultrasound, lymphomas tend to involve dermis and hypodermis with ill-defined borders. They are commonly hypoechoic and present pseudonodular or nodular hypoechoic areas [4, 52, 55].

In cases with panniculitis-like T-cell lymphomas, there is an increase in the hypodermis's echogenicity with hypoechoic thickening of the septa, which can indeed simulate a panniculitis [4, 52, 55, 56].

On color Doppler, they tend to present an intermediate to a high degree of vascularity with low-velocity vessels [4, 55, 56].

Among their differential diagnoses are pseudolymphomas, a heterogeneous group of poly-

clonal reactive lymphoproliferations associated with inflammation. On ultrasound, the borders of nodular pseudolymphomas are usually better defined, and there are [57, 58] hypoechoic globules and teardrop signs within the lesions [59]. Another potential tip for discriminating pseudolymphomas over lymphomas is that in pseudolymphomas, the inflammatory signs (hypervascularity) predominate in the dermis, and their predominant shape is fusiform. In contrast, lymphomas frequently involve the hypodermis, present a higher degree of vascularity than pseudolymphomas, and tend to be ill-defined (Figs. 9.12, 9.13, and 9.14) [59].

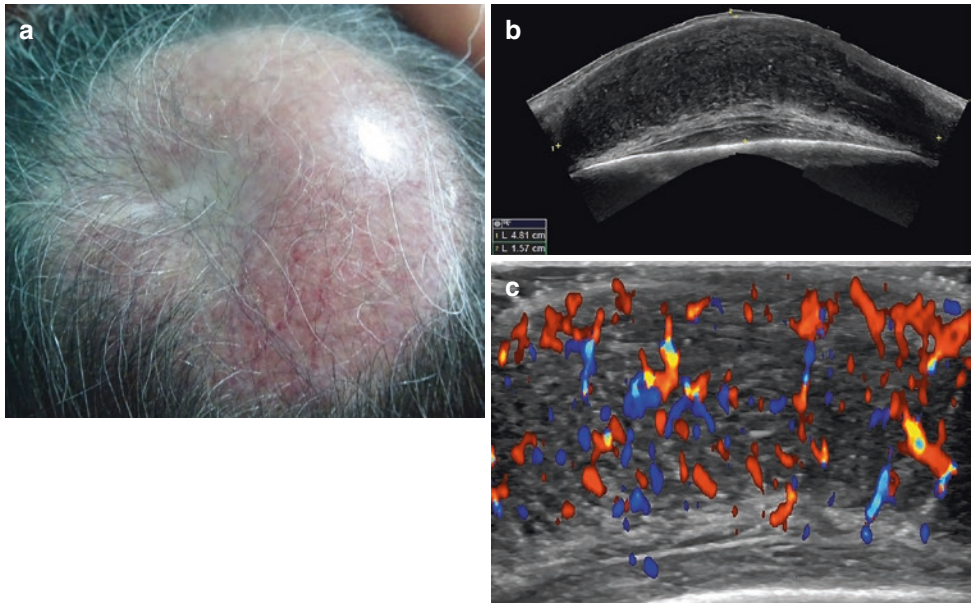

Fig. 9.12 T-cell lymphoma. (**a**) Clinical image of lesion located in the scalp. Ultrasound images (**b**, grayscale; **c**, color Doppler) 4.81 cm (transverse) × 1.57 cm (depth) present hypoechoic and slightly heterogeneous dermal and hypodermal lesion with prominent hypervascularity

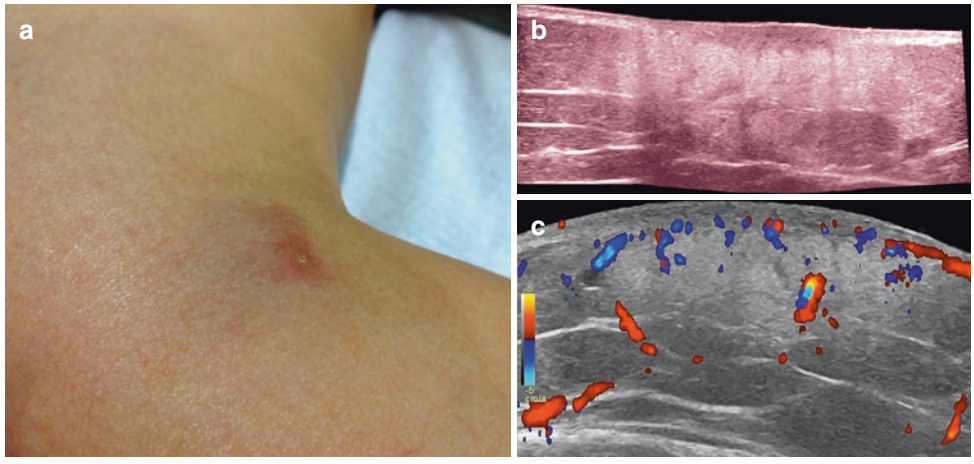

Fig. 9.13 Lymphoma NK panniculitis-like. (**a**) Clinical image in the leg. Ultrasound images (**b**, grayscale with a color filter and **c**, color Doppler; longitudinal views) present thickening and decreased echogenicity of the dermis with increased echogenicity of the hypodermis. There is also slight thickening and hypoechogenicity of the subcutaneous septa. On color Doppler, there is dermal and hypodermal hypervascularity

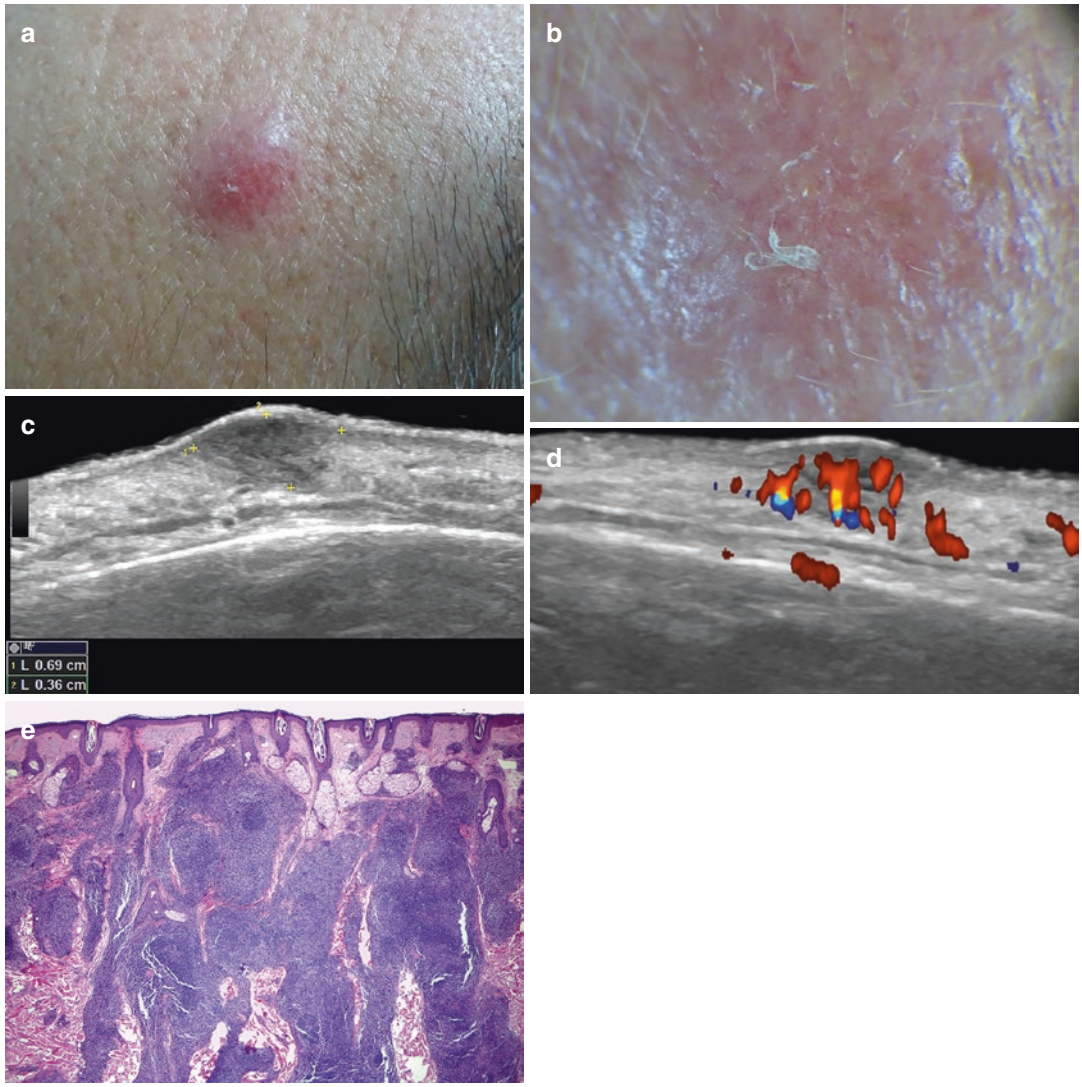

Fig. 9.14 B-cell lymphoma. (**a**) Clinical and (**b**) dermoscopy of lesion located in the frontal region. Ultrasound images (**c**, grayscale and **d**, color Doppler; transverse view) present 0.69 cm (transverse) × 0.36 cm (depth) heterogeneous hypoechoic dermal and hypodermal lesion. On color Doppler, there is prominent hypervascularity within the lesion. (**e**) Histology (H&E 25X): nodular masses of round cell proliferation in the dermis, both superficial and deep, sparing the papillary dermis (Grenz zone) and the epidermis. The lymphoid infiltrates evidence some follicles lacking a well-defined mantle

Liposarcomas

These malignant mesenchymal tumors are composed of lipoblasts and can present a variable appearance [57, 58, 60, 61]. Liposarcoma is the second most common malignant soft-tissue tumor. This entity is pathologically categorized into four subtypes: well-differentiated, myxoid, dedifferentiated, and pleomorphic.

On ultrasound, it has been reported that malignant signs of transformation of lipomas are size >5 cm, heterogeneous echogenicity, ill-defined borders, and hypervascularity. Well-differentiated liposarcomas have been characterized as

isoechoic with tiny hyperechoic lines and hypovascularity. Myxoid liposarcomas present a mix of hypoechoic and anechoic areas with moderate vascularity. Dedifferentiated liposarcomas present a specific biphasic pattern of hyperechoic and hypoechoic areas and hypervascularity. Pleomorphic liposarcomas have been reported to present a specific gyrus-like mixture of hyperechoic and hypoechoic areas (Figs. 9.15 and 9.16) [4, 62].

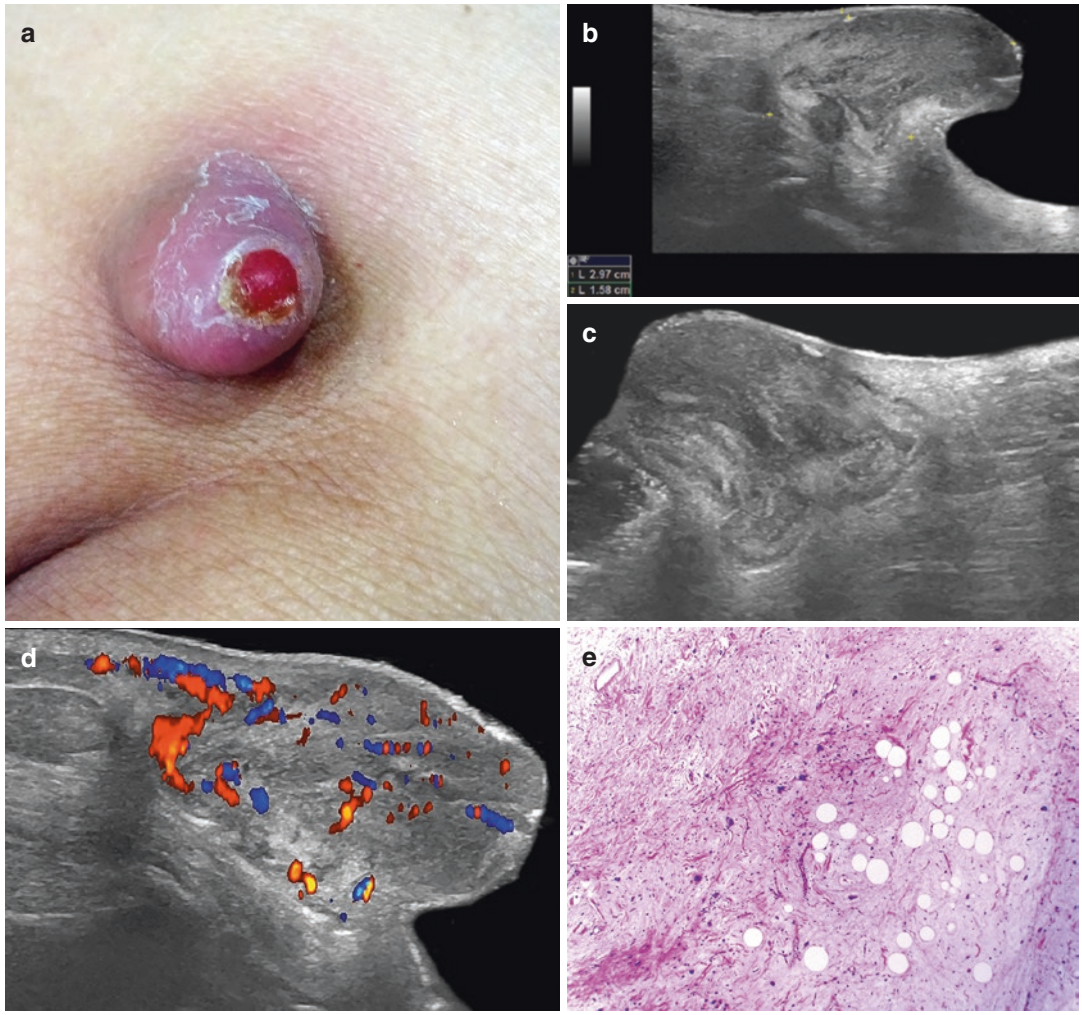

Fig. 9.15 Liposarcoma. (**a**) Clinical image in the lumbosacral region. Ultrasound images (**b** and **c**, grayscale; **b**, longitudinal and **c**; transverse views; **d**, color Doppler) present 2.97 cm (transverse) × 1.58 cm (depth) heterogeneous dermal and hypodermal structure with ill-defined borders, displacing the epidermis upward and with hypervascularity on color Doppler. (**e**) Histology (H&E 100X): a few univacuolated lipoblasts and pleomorphic hyperchromatic lipoblasts are present in a myxoid stroma with hypocellular areas and plexiform slender capillary vessels

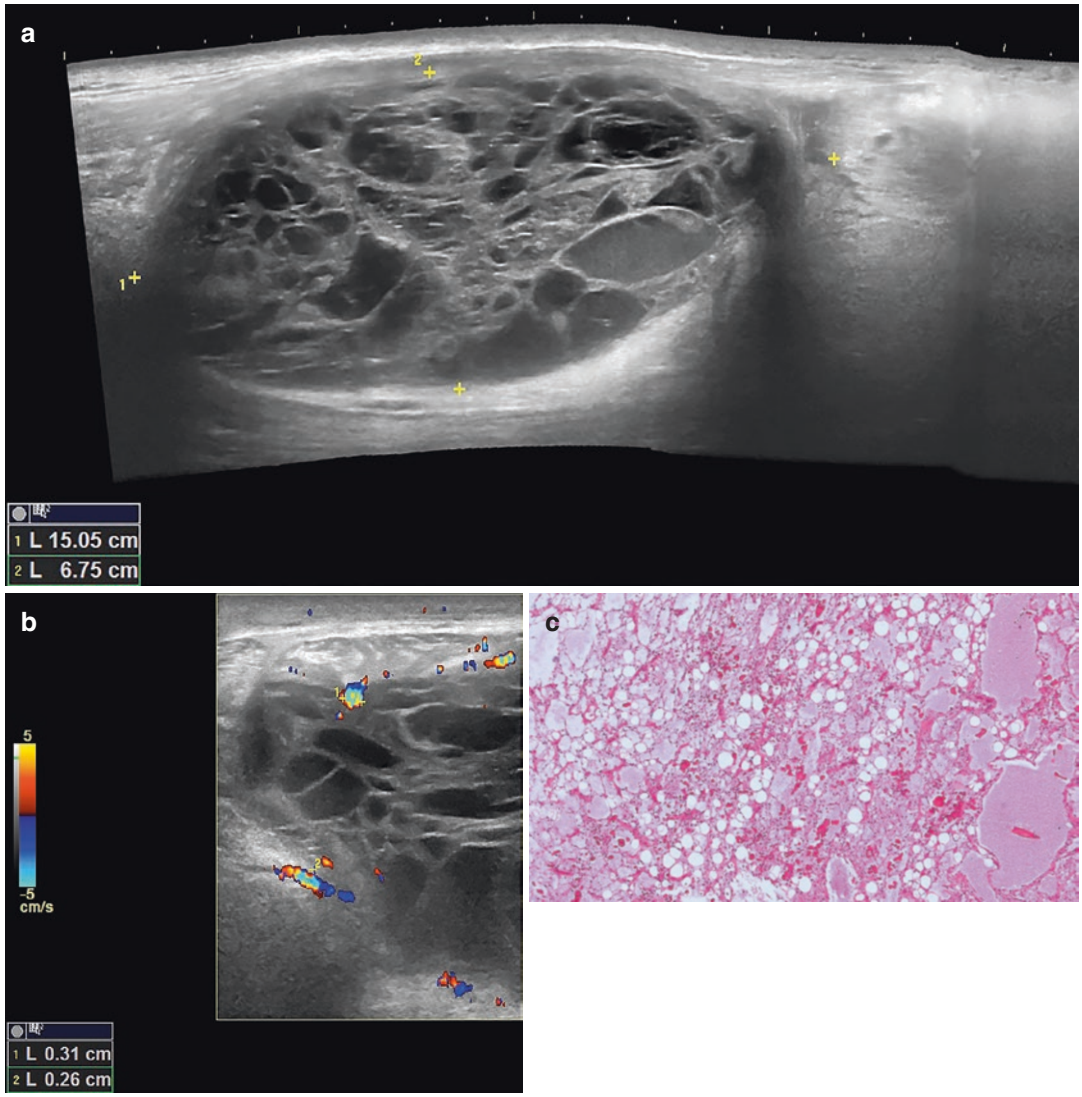

Fig. 9.16 Myxoid liposarcoma. Ultrasound images (**a**, grayscale and **b**, color Doppler; longitudinal views of the posterior aspect of the left thigh) show a 15.05 cm (long) × 6.75 cm (depth) oval-shaped heterogeneous hypodermal structure that contains multiple anechoic pseudocystic areas, septa, and hypoechoic regions. Notice the increased echogenicity of the surrounding hypodermis. On color Doppler, there is slight hypervascularity in the periphery and within some septa. (**c**) Histology (H&E 40x): there is a proliferation of bland spindle cells and myxoid areas with a prominent plexiform ("chicken wire") vasculature

Melanoma

This malignant tumor derived from the melanocytes is the most lethal form of skin cancer [63]. Importantly, ultrasound can provide the thickness of the melanoma (Ultrasonographic Breslow Index) and support the locoregional staging [3, 4, 64–69].

On ultrasound, melanomas are hypoechoic lesions, predominantly fusiform, and involve dermis and/or hypodermis and deeper layers. Nevertheless, in deep melanomas, the shape can be irregular, and there is increased echogenicity of the subcutaneous tissue. Superficial in situ melanomas may not present alterations on ultrasound. If they are located in the acral regions,

sometimes they may generate a loss of the epidermal hyperechoic bilaminar pattern. Keep in mind that among the limitations of ultrasound are the detection of in situ lesions and pigments such as melanin [3, 4, 64–69].

Frequently, melanomas are hypervascular on color Doppler with low-flow arterial and venous vessels (Figs. 9.17, 9.18, and 9.19) [3, 4, 64–69].

Satellite (<2 cm from the primary tumor), in-transit (≥2 cm from the primary tumor), and nodal metastasis can be ruled out with ultrasound [3, 4, 7, 66–85]. The locoregional staging can be performed on ultrasound and starts in the primary tumor or its scar and follows the primary lymphatic drainage regions [3, 4, 7, 67, 69, 70, 72–75, 80, 81, 83, 84]. Satellite and in-transit metastases show as hypoechoic nodules some-

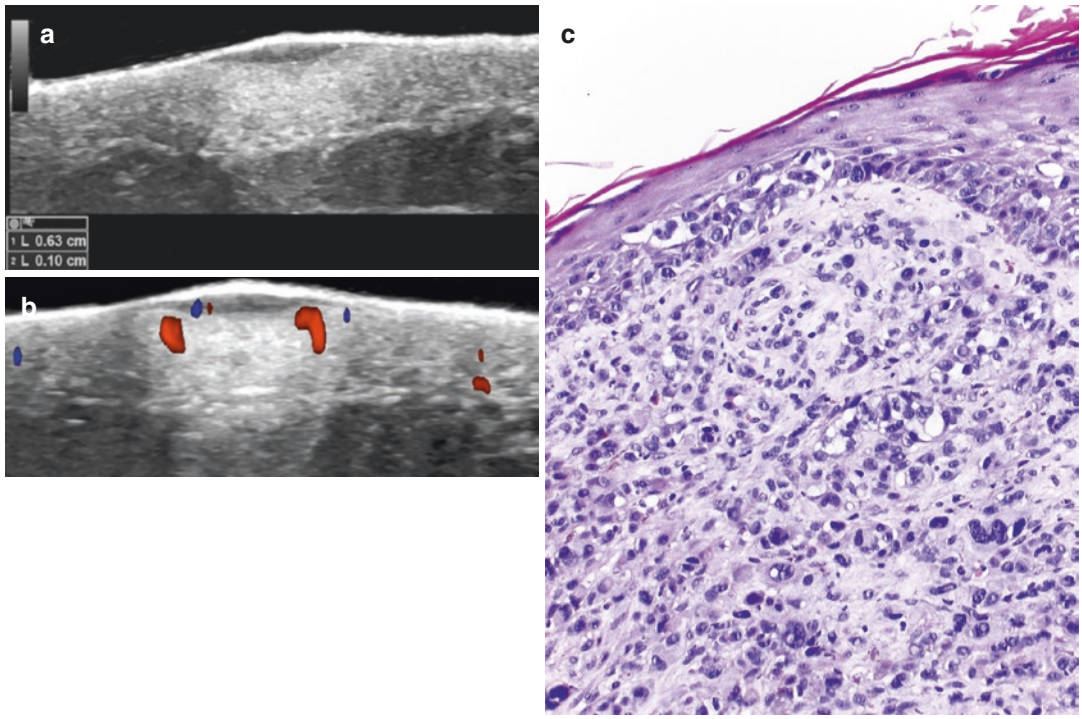

Fig. 9.17 Primary melanoma. Ultrasound images (**a**, grayscale and **b**, color Doppler) show 0.63 cm (transverse) x 0.10 cm (depth) fusiform hypoechoic dermal lesion with hypervascularity. (**c**) Histology (H&E 200X): invasive cutaneous melanoma with atypical melanocytes in the dermis, showing marked nuclear pleomorphism and scant cytoplasmic melanin pigment. Note the presence of pagetoid epidermal involvement by atypical melanocytes above the dermo-epidermal junction

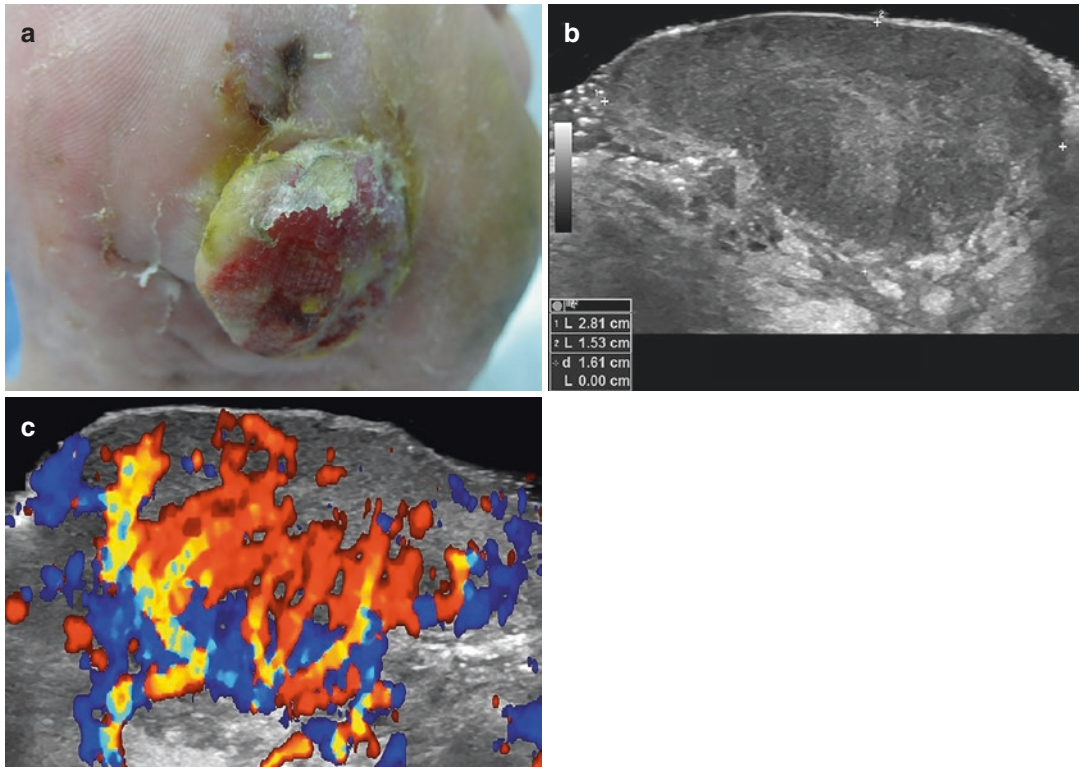

Fig. 9.18 Primary melanoma. (**a**) Clinical lesion in the sole of the left foot. Ultrasound images (**b**, grayscale in transverse view; **c**, color Doppler in longitudinal view) present 2.81 cm (transverse) × 1.53 cm (depth) hypoechoic dermal and hypodermal structure with ill-defined borders. Notice the hyperechogenicity of the subcutaneous tissue in the periphery of the lesion and the high hypervascularity within the structure

times with lobulated borders that present an intermediate or high degree of vascularity (Figs. 9.20, 9.21, 9.22, and 9.23). Occasionally, due to the presence of highly cellular nests of tumoral cells, the metastases may show anechoic areas that do not correspond to necrosis and simulate abscesses. Signs of lymph node infiltration are the change of the shape from oval to round, the loss of the medulla with a fully hypoechoic lymph node, the presence of internal asymmetric hypoechoic nodules in the cortex or medulla, and the cortical and chaotic hypervascularity. The size >1 cm has also been reported as suspicious of malignancy; however, this feature should be added to other signs of malignancy (Fig. 9.24) [3, 4, 7, 67, 69, 70, 72–75, 80, 81, 83, 84].

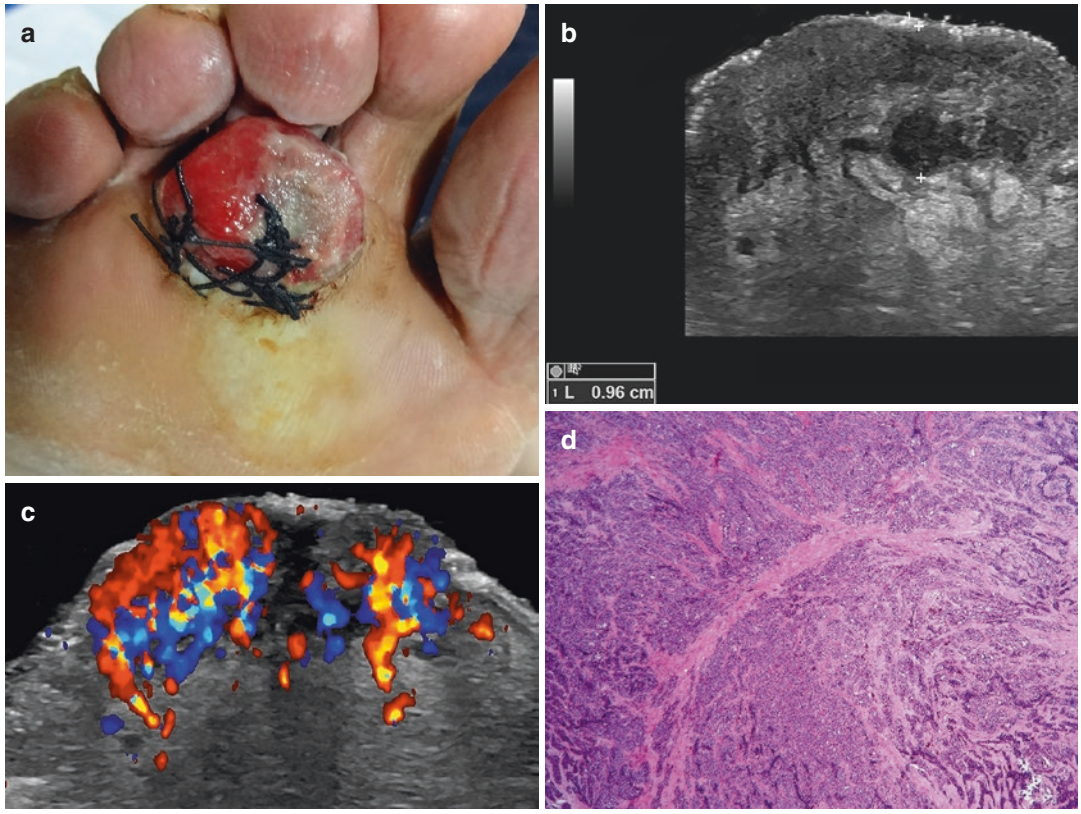

Fig. 9.19 Primary melanoma. (**a**) Clinical lesion. The patient was sent for an ultrasound after the biopsy. Ultrasound images (**b**, grayscale and **c**, color Doppler; transverse views) show ill-defined hypoechoic dermal and hypodermal lesion with ill-defined borders that displaces the epidermis upward. The thickness of the lesion is 0.96 cm. On color Doppler, there is high hypervascularity within the structure and its periphery. (**d**) Histology (H&E 40x): there is a melanocytic proliferation composed of small cells with minimal cytoplasm and round-to-oval hyperchromatic nuclei. Tumor cells are aggregated into elongated expansile nests and diffusely sheeted infiltrates within the fibrous stroma

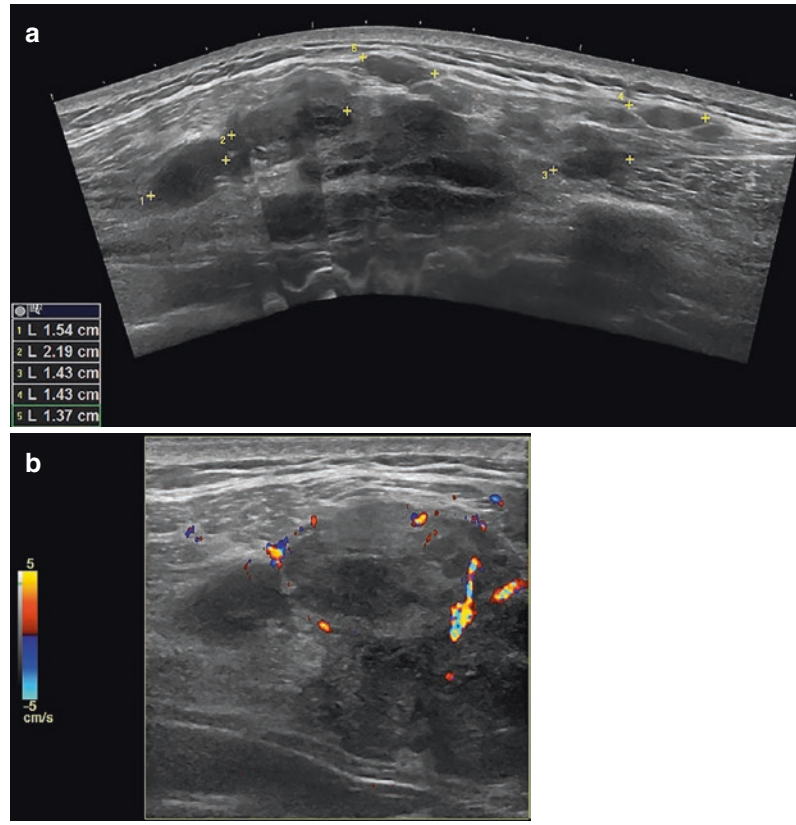

Fig. 9.20 Melanoma metastases. Ultrasound images (**a**, grayscale and **b**, color Doppler; transverse views; left lumbar region) show multiple hypoechoic nodules located in the hypodermis and musculoaponeurotic layers (between markers). On color Doppler, there is increased blood flow in the periphery of the nodules

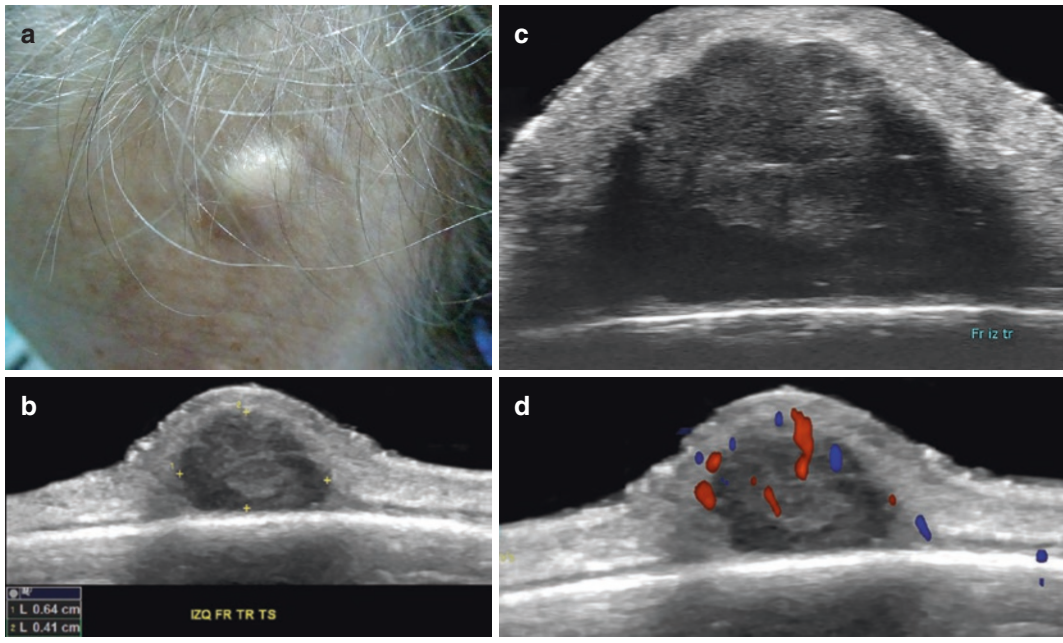

Fig. 9.21 Melanoma metastasis. (**a**) Clinical lesion in the frontal region. Ultrasound images (**a** and **b**, grayscale; **b** at 18 MHz and **c**, at 70 MHz; **d**, color Doppler; transverse views) show 0.64 cm (transverse) × 0.41 cm (depth) hypoechoic dermal and hypodermal nodule with slightly lobulated borders and hypervascularity

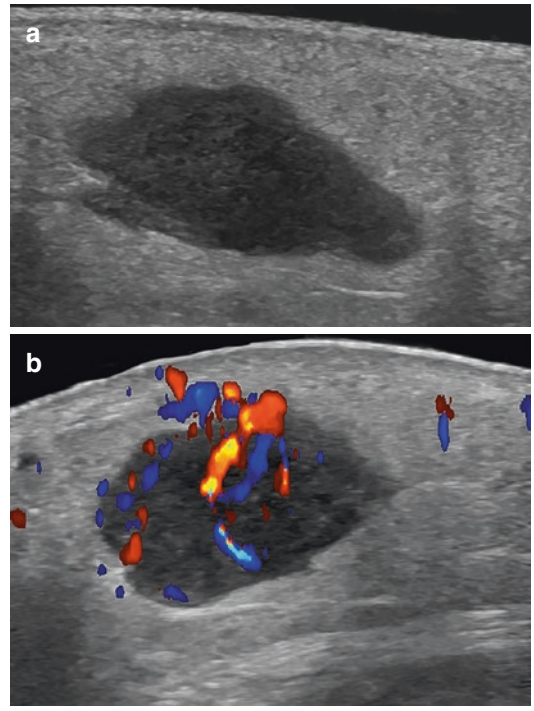

Fig. 9.22 Melanoma metastasis. Ultrasound images (**a**, grayscale; **b**, color Doppler): longitudinal views of the right leg show a hypoechoic oval-shaped hypodermal structure with lobulated borders and increased internal vascularity. Notice the hyperechogenicity of the neighboring subcutaneous tissue

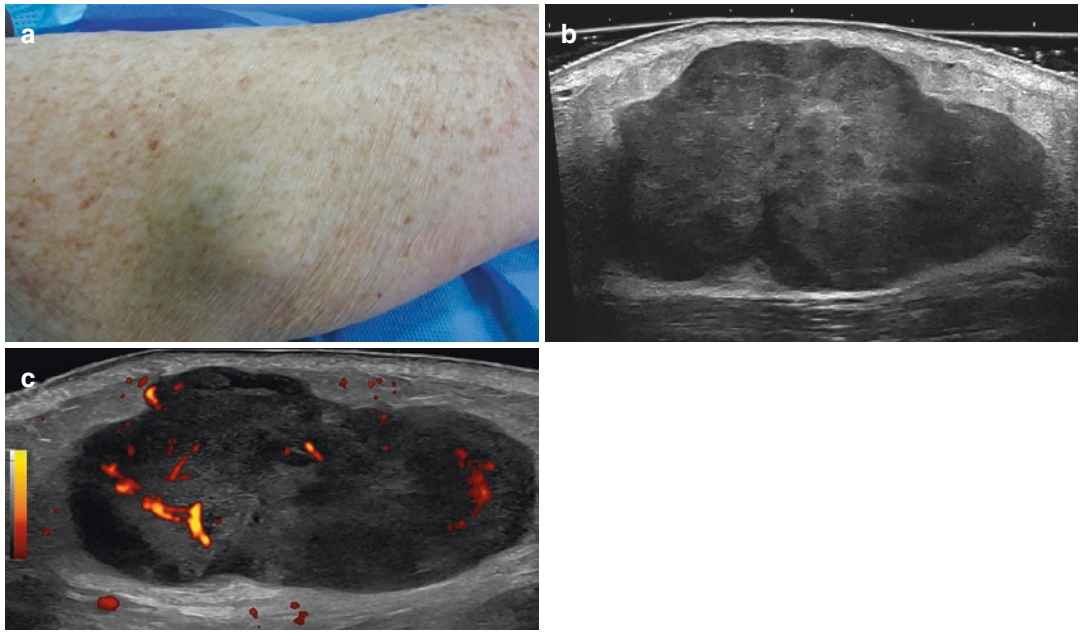

Fig. 9.23 Melanoma metastasis. (**a**) Clinical photograph of a lump in the right arm. Ultrasound images (**b**, grayscale and **c**, power Doppler; longitudinal views) present oval-shaped hypoechoic hypodermal structure with lobulated borders and some small anechoic areas. On color Doppler, there is hypervascularity within the lesion

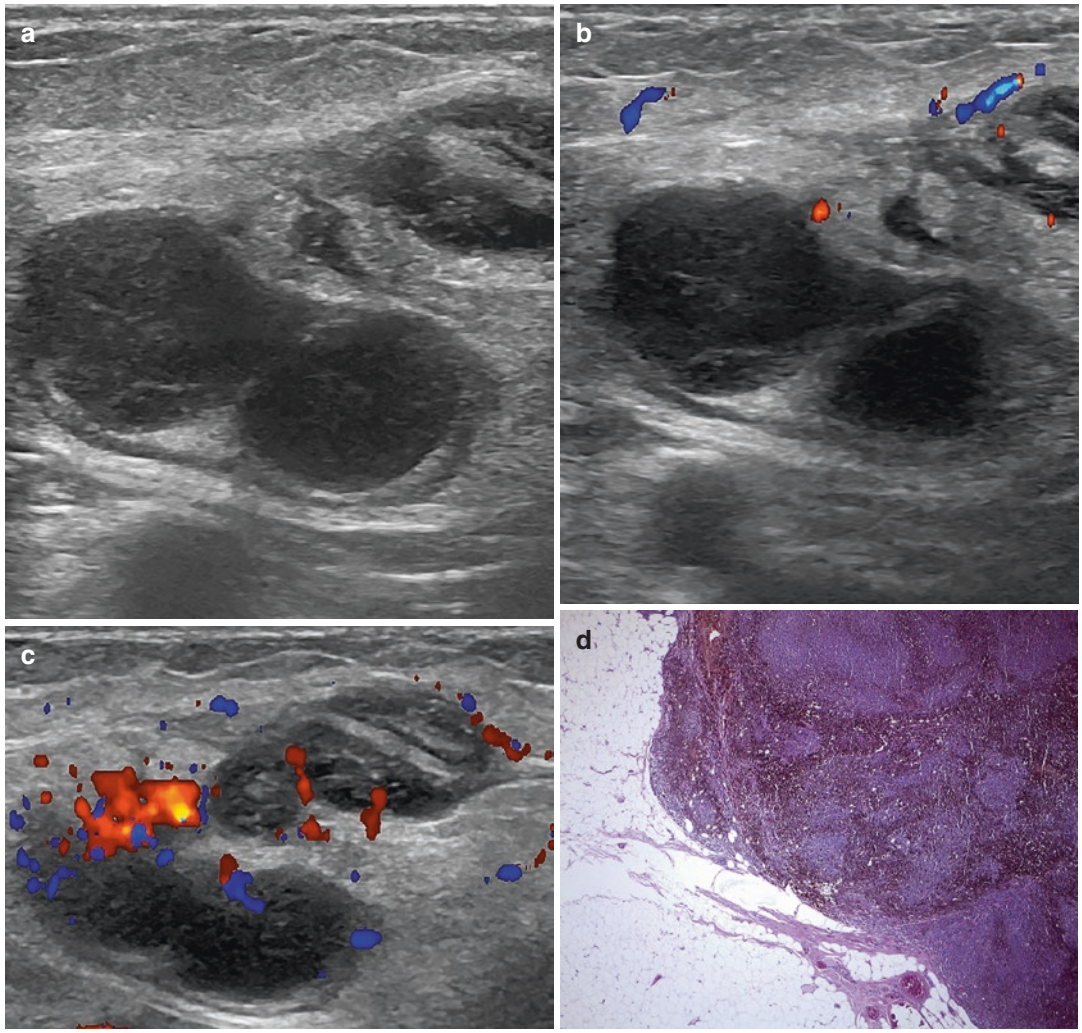

Fig. 9.24 Nodal melanoma metastases. Ultrasound images of infiltrative hypodermal lymph nodes (**a**, gray-scale and **b** and **c**, color Doppler; transverse views) show loss of the hyperechoic medulla and internal nodules within the lymph nodes. There is also an increase in the thickness of the cortex of the lymph nodes. Notice the chaotic hypervascularity of the lymph nodes in **c**. (**d**) Histology (H&E 25X): atypical melanocytes in solid compact masses with irregular melanin distribution, effacing the normal lymph node histoarchitecture

References

1. Wortsman X. Common applications of dermatologic sonography. J Ultrasound Med. 2012;31(1):97–111. https://doi.org/10.7863/jum.2012.31.1.97.
2. Wortsman X. Ultrasound in dermatology: why, how, and when? Semin Ultrasound CT MR. 2013;34(3):177–95. https://doi.org/10.1053/j.sult.2012.10.001.
3. Wortsman X. Atlas of dermatologic ultrasound. First ed. Berlin: Springer International Publishing; 2018. p. 367.
4. Wortsman X, Jemec GBE. Dermatologic ultrasound with clinical and histologic correlations. First ed. New York: Springer-Verlag; 2013.
5. Wortsman X, Wortsman J. Clinical usefulness of variable-frequency ultrasound in localized lesions of the skin. J Am Acad Dermatol. 2010;62(2):247–56. https://doi.org/10.1016/j.jaad.2009.06.016.
6. MacFarlane D, Shah K, Wysong A, Wortsman X, Humphreys TR. The role of imaging in the management of patients with nonmelanoma skin cancer: diagnostic modalities and applications. J Am Acad Dermatol. 2017;76(4):579–88. https://doi.org/10.1016/j.jaad.2015.10.010.

7. Catalano O, Caracò C, Mozzillo N, Siani A. Locoregional spread of cutaneous melanoma: sonography findings. AJR Am J Roentgenol. 2010;194(3):735–45. https://doi.org/10.2214/ajr.09.2422.
8. Ladd ME, Bachert P, Meyerspeer M, et al. Pros and cons of ultra-high-field MRI/MRS for human application. Prog Nucl Magn Reson Spectrosc. 2018;109:1–50. https://doi.org/10.1016/j.pnmrs.2018.06.001.
9. Stahlie EHA, van der Hiel B, Bruining A, et al. The value of lymph node ultrasound and whole body (18) F-FDG PET/CT in stage IIB/C melanoma patients prior to SLNB. Eur J Surg Oncol. 2021;47(5):1157–62. https://doi.org/10.1016/j.ejso.2020.12.007.
10. Twycross SH, Burger H, Holness J. The utility of PET-CT in the staging and management of advanced and recurrent malignant melanoma. S Afr J Surg. 2019;57(3):44–9.
11. Alfageme F, Wortsman X, Catalano O, et al. European Federation of Societies for ultrasound in medicine and biology (EFSUMB) position statement on dermatologic ultrasound. Ultraschall Med. 2021;42(1):39–47. Stellungnahme der European Federation of Societies for Ultrasound in Medicine and Biology (EFSUMB) zu Dermatologischem Ultraschall. https://doi.org/10.1055/a-1161-8872.
12. Wortsman X, Alfageme F, Roustan G, et al. Guidelines for performing dermatologic ultrasound examinations by the DERMUS group. J Ultrasound Med. 2016;35(3):577–80. https://doi.org/10.7863/ultra.15.06046.
13. Dinnes J, Bamber J, Chuchu N, et al. High-frequency ultrasound for diagnosing skin cancer in adults. Cochrane Database Syst Rev. 2018;12(12):CD013188. https://doi.org/10.1002/14651858.CD013188.
14. Barcaui EO, Carvalho ACP, Valiante PM, Piñeiro-Maceira J, Barcaui CB. High-frequency (22-MHz) ultrasound for assessing the depth of basal cell carcinoma invasion. Skin Res Technol. 2021;27(5):676–81. https://doi.org/10.1111/srt.12999.
15. Bezugly A, Rembielak A. The use of high frequency skin ultrasound in non-melanoma skin cancer. J Contemp Brachyther. 2021;13(4):483–91. https://doi.org/10.5114/jcb.2021.108603.
16. Wortsman X. Sonography of facial cutaneous basal cell carcinoma: a first-line imaging technique. J Ultrasound Med. 2013;32(4):567–72. https://doi.org/10.7863/jum.2013.32.4.567.
17. Kwasniak LA, Garcia-Zuazaga J. Basal cell carcinoma: evidence-based medicine and review of treatment modalities. Int J Dermatol. 2011;50(6):645–58. https://doi.org/10.1111/j.1365-4632.2010.04826.x.
18. Lear W, Dahlke E, Murray CA. Basal cell carcinoma: review of epidemiology, pathogenesis, and associated risk factors. J Cutan Med Surg. 2007;11(1):19–30. https://doi.org/10.2310/7750.2007.00011.
19. Qin J, Wang J, Zhu Q, et al. Usefulness of high-frequency ultrasound in differentiating basal cell carcinoma from common benign pigmented skin tumors. Skin Res Technol. 2021;27(5):766–73. https://doi.org/10.1111/srt.13012.
20. Barcaui Ede O, Carvalho AC, Valiante PM, Barcaui CB. High-frequency ultrasound associated with dermoscopy in pre-operative evaluation of basal cell carcinoma. An Bras Dermatol. 2014;89(5):828–31. https://doi.org/10.1590/abd1806-4841.20143176.
21. Bobadilla F, Wortsman X, Muñoz C, Segovia L, Espinoza M, Jemec GB. Pre-surgical high resolution ultrasound of facial basal cell carcinoma: correlation with histology. Cancer Imaging. 2008;8(1):163–72. https://doi.org/10.1102/1470-7330.2008.0026.
22. Coppola R, Barone M, Zanframundo S, et al. Basal cell carcinoma thickness evaluated by high frequency ultrasounds and correlation with dermoscopic features. Ital Dermatol Venereol. 2021;156(5):610–5. https://doi.org/10.23736/s0392-0488.20.06576-1.
23. Hernández-Ibáñez C, Blazquez-Sánchez N, Aguilar-Bernier M, Fúnez-Liébana R, Rivas-Ruiz F, de Troya-Martín M. Usefulness of high-frequency ultrasound in the classification of histologic subtypes of primary basal cell carcinoma. Actas Dermosifiliogr. 2017;108(1):42–51. Utilidad de la ecografía cutánea en la clasificación de subtipos de los carcinomas basocelulares primarios. https://doi.org/10.1016/j.ad.2016.08.002.
24. Khlebnikova A, Molochkov V, Selezneva E, et al. Basal cell carcinoma invasion depth determined with 30 and 75 MHz high-frequency ultrasound and histopathology - a comparative study. Med Ultrason. 2020;22(1):31–6. https://doi.org/10.11152/mu-2233.
25. Khlebnikova AN, Molochkov VA, Selezneva EV, Belova LA, Bezugly A, Molochkov AV. Ultrasonographic features of superficial and nodular basal cell carcinoma. Med Ultrason. 2018;20(4):475–9. https://doi.org/10.11152/mu-1633.
26. Kim HJ, Lee SJ, Lee JH, et al. Usefulness of ultrasonography in determining the surgical excision margin in non-melanocytic skin cancer: a comparative analysis of preoperative ultrasonography and postoperative histopathology. Medicine (Baltimore). 2020;99(51):e23789. https://doi.org/10.1097/md.0000000000023789.
27. Pasquali P, Freites-Martinez A, Fortuño-Mar A. Ex vivo high-frequency ultrasound: a novel proposal for management of surgical margins in patients with non-melanoma skin cancer. J Am Acad Dermatol. 2016;74(6):1278–80. https://doi.org/10.1016/j.jaad.2016.01.006.
28. Piłat P, Borzęcki A, Jazienicki M, Gerkowicz A, Krasowska D. High-frequency ultrasound in the diagnosis of selected non-melanoma skin nodular lesions. Postepy Dermatol Alergol. 2019;36(5):572–80. https://doi.org/10.5114/ada.2019.89505.
29. Vilas-Sueiro A, Alfageme F, Salgüero I, De Las HC, Roustan G. Ex vivo high-frequency ultrasound for assessment of basal cell carcinoma. J Ultrasound

Med. 2019;38(2):529–31. https://doi.org/10.1002/jum.14706.
30. Wang LF, Zhu AQ, Wang Q, et al. Value of high-frequency ultrasound for differentiating invasive basal cell carcinoma from non-invasive types. Ultrasound Med Biol. 2021;47(10):2910–20. https://doi.org/10.1016/j.ultrasmedbio.2021.06.006.
31. Wang SQ, Liu J, Zhu QL, et al. High-frequency ultrasound features of basal cell carcinoma and its association with histological recurrence risk. Chin Med J (Engl). 2019;132(17):2021–6. https://doi.org/10.1097/cm9.0000000000000369.
32. Wortsman X. Ultrasound diagnosis of infiltrative versus noninfiltrative subtypes of cutaneous basal cell carcinoma. J Ultrasound Med. 2019;38(11):3083. https://doi.org/10.1002/jum.14994.
33. Wortsman X, Vergara P, Castro A, et al. Ultrasound as predictor of histologic subtypes linked to recurrence in basal cell carcinoma of the skin. J Eur Acad Dermatol Venereol. 2015;29(4):702–7. https://doi.org/10.1111/jdv.12660.
34. Navarrete-Dechent C, Liopyris K, Rishpon A, et al. Association of Multiple aggregated yellow-white globules with nonpigmented basal cell carcinoma. JAMA Dermatol. 2020;156(8):882–90. https://doi.org/10.1001/jamadermatol.2020.1450.
35. Vega N, Wortsman X, Navarrete N, Sazunic I. Color Doppler ultrasound supports early diagnosis of mixed high and low risk of recurrence subtypes in the same basal cell carcinoma lesion. Dermatol Surg. 2018;44(5):741–3. https://doi.org/10.1097/dss.0000000000001328.
36. Zhu AQ, Wang LF, Li XL, et al. High-frequency ultrasound in the diagnosis of the spectrum of cutaneous squamous cell carcinoma: noninvasively distinguishing actinic keratosis, Bowen's Disease, and invasive squamous cell carcinoma. Skin Res Technol. 2021;27(5):831–40. https://doi.org/10.1111/srt.13028.
37. Mujtaba B, Wang F, Taher A, et al. Dermatofibrosarcoma protuberans: pathological and imaging review. Curr Probl Diagn Radiol. 2021;50(2):236–40. https://doi.org/10.1067/j.cpradiol.2020.05.011.
38. Shin YR, Kim JY, Sung MS, Jung JH. Sonographic findings of dermatofibrosarcoma protuberans with pathologic correlation. J Ultrasound Med. 2008;27(2):269–74. https://doi.org/10.7863/jum.2008.27.2.269.
39. Zou MH, Huang Q, Yang T, et al. Role of ultrasound in the diagnosis of primary and recurrent dermatofibrosarcoma protuberans. BMC Cancer. 2021;21(1):909. https://doi.org/10.1186/s12885-021-08476-2.
40. Catalano O, Alfageme Roldán F, Scotto di Santolo M, Solivetti FM, Wortsman X. Color Doppler sonography of Merkel cell carcinoma. J Ultrasound Med. 2018;37(1):285–92. https://doi.org/10.1002/jum.14329.
41. Hernández-Aragüés I, Vázquez-Osorio I, Alfageme F, et al. Skin ultrasound features of Merkel cell carcinoma. J Eur Acad Dermatol Venereol. 2017;31(7):e315–8. https://doi.org/10.1111/jdv.14102.
42. Lemos BD, Storer BE, Iyer JG, et al. Pathologic nodal evaluation improves prognostic accuracy in Merkel cell carcinoma: analysis of 5823 cases as the basis of the first consensus staging system. J Am Acad Dermatol. 2010;63(5):751–61. https://doi.org/10.1016/j.jaad.2010.02.056.
43. Ramahi E, Choi J, Fuller CD, Eng TY. Merkel cell carcinoma. Am J Clin Oncol. 2013;36(3):299–309. https://doi.org/10.1097/COC.0b013e318210f83c.
44. Akaike G, Akaike T, Fadl SA, Lachance K, Nghiem P, Behnia F. Imaging of Merkel cell carcinoma: what imaging experts should know. Radiographics. 2019;39(7):2069–84. https://doi.org/10.1148/rg.2019190102.
45. Singh N, Alexander NA, Lachance K, et al. Clinical benefit of baseline imaging in Merkel cell carcinoma: analysis of 584 patients. J Am Acad Dermatol. 2021;84(2):330–9. https://doi.org/10.1016/j.jaad.2020.07.065.
46. Dummer R, Vermeer MH, Scarisbrick JJ, et al. Cutaneous T cell lymphoma. Nat Rev Dis Primers. 2021;7(1):61. https://doi.org/10.1038/s41572-021-00296-9.
47. Kempf W, Mitteldorf C. Cutaneous T-cell lymphomas-an update 2021. Hematol Oncol. 2021;39(Suppl 1):46–51. https://doi.org/10.1002/hon.2850.
48. Lang CCV, Ramelyte E, Dummer R. Innovative therapeutic approaches in primary cutaneous B cell lymphoma. Front Oncol. 2020;10:1163. https://doi.org/10.3389/fonc.2020.01163.
49. Zic JA. Diagnosis and management of cutaneous lymphomas including cutaneous T-cell lymphoma. Med Clin North Am. 2021;105(4):737–55. https://doi.org/10.1016/j.mcna.2021.04.010.
50. Vitiello P, Sica A, Ronchi A, Caccavale S, Franco R, Argenziano G. Primary cutaneous B-cell lymphomas: an update. Front Oncol. 2020;10:651. https://doi.org/10.3389/fonc.2020.00651.
51. Malachowski SJ, Sun J, Chen PL, Seminario-Vidal L. Diagnosis and management of cutaneous B-cell lymphomas. Dermatol Clin. 2019;37(4):443–54. https://doi.org/10.1016/j.det.2019.05.004.
52. Specht L, Skov L. Cutaneous lymphomas. Clin Oncol (R Coll Radiol). 2019;31(11):797–807. https://doi.org/10.1016/j.clon.2019.07.018.
53. Vaidya T, Badri T. Mycosis fungoides. Treasure Island (FL): StatPearls. StatPearls Publishing. Copyright © 2021, StatPearls Publishing LLC; 2021.
54. Musick SR, Lynch DT. Subcutaneous Panniculitis Like T-cell Lymphoma. Treasure Island (FL): StatPearls. StatPearls Publishing Copyright © 2021, StatPearls Publishing LLC; 2021.

55. Mandava A, Koppula V, Wortsman X, Catalano O, Alfageme F. The clinical value of imaging in primary cutaneous lymphomas: role of high resolution ultrasound and PET-CT. Br J Radiol. 2019;92(1095):20180904. https://doi.org/10.1259/bjr.20180904.
56. Polańska A, Dańczak-Pazdrowska A, Olek-Hrab K, et al. High-frequency ultrasonography-new non-invasive method in assessment of skin lymphomas. Skin Res Technol. 2018;24(3):517–21. https://doi.org/10.1111/srt.12450.
57. Mentzel T, Palmedo G, Hantschke M, Woziwodzki J, Beck C. Mixed-type liposarcoma: clinicopathological, immunohistochemical, and molecular analysis of a case arising in deep soft tissues of the lower extremity. Virchows Arch. 2008;453(2):197–201. https://doi.org/10.1007/s00428-008-0624-7.
58. Morag Y, Yablon C, Brigido MK, Jacobson J, Lucas D. Imaging appearance of well-differentiated liposarcomas with myxoid stroma. Skelet Radiol. 2018;47(10):1371–82. https://doi.org/10.1007/s00256-018-2940-6.
59. Wortsman X, Ferreira-Wortsman C, Pizarro K, Morales C. Ultrasonography of cutaneous nodular pseudolymphoma at 18 and 71 MHz. Skin Res Technol. 2021;28(1):176–9. https://doi.org/10.1111/srt.13099.
60. Renn A, Adejolu M, Messiou C, et al. Overview of malignant soft-tissue sarcomas of the limbs. Clin Radiol. 2021;76(12):940.e1–940.e16. https://doi.org/10.1016/j.crad.2021.08.011.
61. Zafar R, Wheeler Y. Liposarcoma. Treasure Island (FL): StatPearls. StatPearls Publishing Copyright © 2021, StatPearls Publishing LLC; 2021.
62. Shimamori N, Kishino T, Morii T, et al. Sonographic appearances of Liposarcoma: correlations with pathologic subtypes. Ultrasound Med Biol. 2019;45(9):2568–74. https://doi.org/10.1016/j.ultrasmedbio.2019.05.020.
63. Leonardi GC, Falzone L, Salemi R, et al. Cutaneous melanoma: from pathogenesis to therapy (review). Int J Oncol. 2018;52(4):1071–80. https://doi.org/10.3892/ijo.2018.4287.
64. Belfiore MP, Reginelli A, Russo A, et al. Usefulness of high-frequency ultrasonography in the diagnosis of melanoma: mini review. Front Oncol. 2021;11:673026. https://doi.org/10.3389/fonc.2021.673026.
65. Crisan M, Crisan D, Sannino G, Lupsor M, Badea R, Amzica F. Ultrasonographic staging of cutaneous malignant tumors: an ultrasonographic depth index. Arch Dermatol Res. 2013;305(4):305–13. https://doi.org/10.1007/s00403-013-1321-1.
66. Nazarian LN, Alexander AA, Rawool NM, Kurtz AB, Maguire HC, Mastrangelo MJ. Malignant melanoma: impact of superficial US on management. Radiology. 1996;199(1):273–7. https://doi.org/10.1148/radiology.199.1.8633159.
67. Piłat P, Borzęcki A, Jazienicki M, Gerkowicz A, Szubstarski F, Krasowska D. Evaluation of the clinical usefulness of high-frequency ultrasonography in pre-operative evaluation of cutaneous melanoma - a prospective study. Postepy Dermatol Alergol. 2020;37(2):207–13. https://doi.org/10.5114/ada.2018.79939.
68. Reginelli A, Belfiore MP, Russo A, et al. A preliminary study for quantitative assessment with HFUS (high- frequency ultrasound) of nodular skin melanoma Breslow thickness in adults before surgery: interdisciplinary team experience. Curr Radiopharm. 2020;13(1):48–55. https://doi.org/10.2174/1874471012666191007121626.
69. Wortsman X. Sonography of the primary cutaneous melanoma: a review. Radiol Res Pract. 2012;2012:814396. https://doi.org/10.1155/2012/814396.
70. Adibelli ZH, Unal G, Gül E, Uslu F, Koçak U, Abali Y. Differentiation of benign and malignant cervical lymph nodes: value of B-mode and color Doppler sonography. Eur J Radiol. 1998;28(3):230–4. https://doi.org/10.1016/s0720-048x(97)00174-5.
71. Álvarez-Chinchilla P, Encabo-Duran B, Poveda I, Planelles M, Bañuls J. Cutaneous metastases of melanoma presenting as sudden haematomas: clinical, dermoscopic and sonographic features. Clin Exp Dermatol. 2018;43(7):852–4. https://doi.org/10.1111/ced.13667.
72. Catalano O. Critical analysis of the ultrasonographic criteria for diagnosing lymph node metastasis in patients with cutaneous melanoma: a systematic review. J Ultrasound Med. 2011;30(4):547–60. https://doi.org/10.7863/jum.2011.30.4.547.
73. Catalano O, Setola SV, Vallone P, Raso MM, D'Errico AG. Sonography for locoregional staging and follow-up of cutaneous melanoma: how we do it. J Ultrasound Med. 2010;29(5):791–802. https://doi.org/10.7863/jum.2010.29.5.791.
74. Catalano O, Voit C, Sandomenico F, et al. Previously reported sonographic appearances of regional melanoma metastases are not likely due to necrosis. J Ultrasound Med. 2011;30(8):1041–9. https://doi.org/10.7863/jum.2011.30.8.1041.
75. Chang DB, Yuan A, Yu CJ, Luh KT, Kuo SH, Yang PC. Differentiation of benign and malignant cervical lymph nodes with color Doppler sonography. AJR Am J Roentgenol. 1994;162(4):965–8. https://doi.org/10.2214/ajr.162.4.8141027.
76. Dragoni F, Cartoni C, Pescarmona E, et al. The role of high resolution pulsed and color Doppler ultrasound in the differential diagnosis of benign and malignant lymphadenopathy: results of multivariate analysis. Cancer. 1999;85(11):2485–90. https://doi.org/10.1002/(sici)1097-0142(19990601)85:11<2485::aid-cncr26>3.0.co;2-y.
77. Faita F, Oranges T, Di Lascio N, et al. Ultra-high-frequency ultrasound and machine learning approaches for the differential diagnosis of melanocytic lesions. Exp Dermatol. 2022;31(1):94–8. https://doi.org/10.1111/exd.14330.

78. Lassau N, Mercier S, Koscielny S, et al. Prognostic value of high-frequency sonography and color Doppler sonography for the preoperative assessment of melanomas. AJR Am J Roentgenol. 1999;172(2):457–61. https://doi.org/10.2214/ajr.172.2.9930803.
79. Lassau N, Spatz A, Avril MF, et al. Value of high-frequency US for preoperative assessment of skin tumors. Radiographics. 1997;17(6):1559–65. https://doi.org/10.1148/radiographics.17.6.9397463.
80. Nazarian LN, Alexander AA, Kurtz AB, et al. Superficial melanoma metastases: appearances on gray-scale and color Doppler sonography. AJR Am J Roentgenol. 1998;170(2):459–63. https://doi.org/10.2214/ajr.170.2.9456964.
81. Nijhuis A, Chung D, London K, Uren R, Thompson J, Nieweg O. Ultrasound examination of the lymphatic drainage area and regional lymph nodes in melanoma patients with in-transit metastases. Ann Surg Oncol. 2021;28(3):1625–31. https://doi.org/10.1245/s10434-020-09240-9.
82. Nijhuis AAG, Spillane AJ, Stretch JR, et al. Current management of patients with melanoma who are found to be sentinel node-positive. ANZ J Surg. 2020;90(4):491–6. https://doi.org/10.1111/ans.15491.
83. Prkačin I, Šitum M, Delaš Aždajić M, Puljiz Z. Ultrasound assessment of regional lymph nodes in melanoma staging. Acta Dermatovenerol Croat. 2021;29(2):80–7.
84. Voit C, Van Akkooi AC, Schäfer-Hesterberg G, et al. Ultrasound morphology criteria predict metastatic disease of the sentinel nodes in patients with melanoma. J Clin Oncol. 2010;28(5):847–52. https://doi.org/10.1200/jco.2009.25.7428.
85. Ying M, Bhatia KS, Lee YP, Yuen HY, Ahuja AT. Review of ultrasonography of malignant neck nodes: greyscale, Doppler, contrast enhancement and elastography. Cancer Imaging. 2014;13(4):658–69. https://doi.org/10.1102/1470-7330.2013.0056.